
Article:
Longhi, M.A., Rodríguez, E.D., Walkley, B. orcid.org/0000-0003-1069-1362 et al. (2 more authors) (2020) Metakaolin-based geopolymers: Relation between formulation, physicochemical properties and efflorescence formation. Composites Part B: Engineering, 182. 107671. ISSN 1359-8368

https://doi.org/10.1016/j.compositesb.2019.107671

Metakaolin-based geopolymers: relation between formulation, physicochemical properties and efflorescence formation

Márlon A. Longhi[a, b*], Erich D. Rodríguez[c], Brant Walkley[d,e], Zuhua Zhang[b,f*], Ana Paula Kirchheim[a]

[a]Building Innovation Research Unit, Universidade Federal do Rio Grande do Sul (NORIE/UFRGS), Av. Osvaldo Aranha, 99. 3ºandar, Porto Alegre, Brazil

[b]Centre for Future Materials, University of Southern Queensland, Toowoomba, QLD 4350, Australia.

[c]Department of Structures and Civil Construction. Technology Centre, Universidade Federal de Santa Maria, Santa Maria, Av. Roraima 1000. Prédio 7. RS, Brazil.

[d]Department of Materials Science and Engineering, Sir Robert Hadfield Building, The University of Sheffield, Sheffield S1 3JD, United Kingdom.

[e]Department of Chemical and Biological Engineering, Sir Robert Hadfield Building, The University of Sheffield, Sheffield S1 3JD, United Kingdom.

[f]Key Laboratory for Green & Advanced Civil Engineering Materials and Application Technology of Hunan Province, College of Civil Engineering, Hunan University, Changsha 410082, PR China.

ABSTRACT

The efflorescence formation in metakaolin-based geopolymers is assessed in this study to provide a better understanding of the effect of the synthesis parameters. Efflorescence formation depends on the physical and chemical properties of geopolymers as well as the environmental exposure conditions. In this study a set of fifteen geopolymers were synthesized using different formulation. An accelerated test of efflorescence development is presented, where the grade of degradation was evaluated by visual observation and correlated to leaching potential, physical properties and microstructural features. The use of soluble silicate in the activator provides a denser and a less permeable matrix.

This makes the extraction of free alkalis to the surface more difficult, reducing the extent of alkali leaching and therefore efflorescence. The use of K^+ is also effective to reduce visible efflorescence. The efflorescence formation is predicted by the properties of the gel formed which are dependent on the mix proportioning.

KEYWORDS: Alkali-activated cement (AAC); geopolymer; metakaolin; efflorescence; leaching.

1. INTRODUCTION

Geopolymer cements are engineered, sustainable alternatives to Portland cements that have proven, large scale application in civil construction [1–4]. These materials are well recognized in terms of mechanical performance and lower environmental impact resulting from low carbon dioxide (CO_2) emissions [2,3,5–10]. However, their widespread implementation remains limited due to lack of large availability, homogeneous, low cost and feasible raw materials in some regions, lack of international standards for their production and characterization, as well as an incomplete understanding of their durability properties in regard to alkali-aggregate reaction, carbonation, acid attack and efflorescence, and the underlying physicochemical interactions governing this behaviour [3].

Therefore, enhanced durability is one of the key drivers for adoption of this technology. There has been significant focus on understanding geopolymer durability when these materials were exposed to several aggressive environments (marine conditions, sulfate exposure and chloride ingress) and carbonation conditions [11–17]. However, the mix proportioning controlling the susceptibility of geopolymers to leaching of alkalis when exposed to water and subsequent efflorescence is still not fully understood. In particular, an effective methodology for efflorescence elimination remains absent from the literature [18].

Efflorescence results from leaching of free alkalis present in the pore structure when in contact with water. These leached alkalis then react with carbonic acid (formed by dissolution of atmospheric carbon dioxide), forming alkali salts which crystallize on the geopolymer surface [18–21]. Alkali salt crystals can also form within the pore network underneath the surface due to diffusion of dissolved CO_3^{2-} ions, that is a phenomenon named by Zhang et al. [22] as subflorescence. Efflorescence is also observed in Portland cement [23], however the higher concentrations of alkalis in geopolymer cements (the excess of which may not be chemically bound in the gel structure) makes them particularly susceptible to this phenomenon. Previous work has shown that the movement of free alkalis in the pore solution (resulting from excess, weakly-bonded or unreacted alkalis) and extraction

of these alkalis during leaching is influenced by the pore structure, where a denser and more tortuous pore network impedes movement of the alkali cations [12,15,19,22,24–26]. Physical and chemical properties, which are related to formation of efflorescence, are dependent on geopolymer mix proportioning and synthesis conditions. This relation is complex due to the wide number of parameters, which directly affect the susceptibility of efflorescence formation. Although efflorescence development has been assessed in different fly ash and pozzolan-based geopolymers [12,25,26], its consequences and effects remain poorly understood, and will be evaluated in more detail in this work.

Geopolymers contain a pseudo-zeolitic three-dimensional aluminosilicate network comprising SiO_4 and AlO_4 tetrahedra. The negative charge arising from the substitution of Al^{3+} for Si^{4+} in tetrahedral coordination is compensated by an alkali cation (commonly Na^+ or K^+ from the activator) [27]. Therefore, the maximum content of Na^+ bound to the gel framework is defined by the molar ratio Al_2O_3/Na_2O close to the unit. Sodium can also be partially associated in the form of $Na(H_2O)_n^+$ with Na^+ in a hydrogen bond [27] and associated with a framework oxygen bonds [28]. Excessive alkali ions are present in the pore solution and are not chemically bound [29] as a consequence of a high dosage in the activator and/or presence of non-soluble Al_2O_3. The amount of geopolymer gel formed, its structure, tortuosity of the pore network and the consequent susceptibility of the geopolymer cement to alkali leaching is also dependent on the reactivity degree of the precursor (which results in the presence of excess alkalis) [22]. On the same way, the reaction degree is dependent on the curing conditions (temperature, time and humidity) and the amount alkalis and soluble silicate in the activator [20,25]. The high content of alkalis used during activation can result in substantial leaching of the excess alkalis, with leaching of between 7 and 16 wt. % of the total alkalis as observed in previous studies [12,25] and can reach potential values greater than 50 wt.% to metakaolin-based geopolymers [21]. This can result in removal of alkalis from both the pore network and gel framework and affecting the geopolymer service life aesthetically due to the visual efflorescence formation or superficial deterioration and mechanically due to the reduction in compressive strength [22,26]. In previous work, it was demonstrated that this deleterious process promotes significant changes in the chemical environment of the Al present in the geopolymer gel. The removal of alkalis induces the

reduction of $Q^4(4Al)$ and Al(VI) species as observed by ^{29}Si and ^{27}Al MAS-NMR and FTIR analysis [21].

Despite the recent advances in understanding efflorescence formation, there remains an absence of knowledge about the fundamental relationships between precursor chemistry, reaction mix proportioning, gel microstructure and efflorescence. This knowledge can only be obtained through a systematic study varying design parameters in a simplified model system. Previous studies have primarily examined geopolymer cements produced from highly chemically and physically heterogeneous industrial by-products such as fly ashes and granulated blast furnace slag [12,15,19,22,24–26]. In contrast, metakaolin derived from high purity kaolinitic clays exhibits a Si/Al ratio close to 1.0, high purity and reactivity, and provides a reliable and reproducible precursor for production of high purity geopolymers.

In the study presented here, the efflorescence formation is evaluated in a series of metakaolin-based geopolymers with systematic variation of alkali and soluble silicate contents, and is then correlated with the physical, chemical and microstructural features of the gel.

2. EXPERIMENTAL PROGRAM

2.1 Materials and sample preparation

A commercial metakaolin (MetaMax – BASF) was used as the aluminosilicate precursor. The metakaolin has a mean particle size of 4.56 μm, specific surface area of 13.49 kg/m² and an oxide composition of 54.82% wt.% SiO_2, 42.57 wt.% Al_2O_3, 1.23 wt.% TiO_2, 0.48 wt.% Fe_2O_3 with 0.11 wt.% loss of ignition at 1000 °C. The particle morphology is shown in Figure 1. This material exhibits a smaller particle size than other calcined clays used as a geopolymer precursor in previous studies [30,31], which results in a higher water consumption during geopolymer production.

The alkali activating solutions were prepared by initially mixing sodium hydroxide pellets (NaOH: ~99%, Chem-Supply, Australia) with distilled water to form a sodium hydroxide solution, and

subsequently mixing this sodium hydroxide solution with a commercial sodium silicate solution (29.4 wt.% SiO_2, 14.7 wt.% Na_2O, and 55.9 wt.% H_2O, PQ, Australia) in proportions to reach the desired molar ratios.

Geopolymer mixes were formulated with different alkali contents (represented by M_2O = 15, 20 and 25 wt.%), using Na^+ as main alkali and partial K^+ in some mixtures. The content of soluble silicate in the activator (expressed by the modulus of silica MS, the SiO_2/M_2O molar ratio in the activator) was varied such that MS = 0.0, 0.5 and 1.0. The geopolymers were cured at either ambient temperature (~25 °C) and relative humidity (RH) ≥ 90% or at 50 °C. The increasing of temperature was made in an oven, with a hermetically sealed box with water in the bottom, without contact with the samples. This process provides a high humidity (RH>95%) and avoid the loss of water by evaporation. The geopolymers were identified according to the content of sodium (H- high, 25%; M-medium, 20% and L- low, 15%) or sodium and potassium (Na+K) and the MS modulus (0.0, 0.5 and 1.0). The mix proportioning of the geopolymers and their resulting compressive strength (testing details are provided below) are shown in Table 1. It is important to highlight that the geopolymers were designed to provide different mechanical and physical properties to allow it's correlation with efflorescence formation. According to this, the compressive strength was evaluated as mechanical properties, and the dosage was not intended to improve this property, where is possible to observe values between 1 to 45 MPa.

Pastes were mixed for 5 min using a mechanical mixer (285 rpm) and then were poured into moulds. After one day at either 25 or 50 °C, the samples were removed from the moulds, sealed with plastic film and stored during 27 days in room temperature (~25 °C) and RH ≥ 90% controlled during 24 h per day.

2.2 Tests conducted

The efflorescence formation was assessed by visual observation of the samples after curing for 28 days. The environmental conditions were controlled at 20 ± 5 °C and RH of 65 ± 20%. The samples were subsequently subjected to two different conditions, as follows: (i) partial immersion in 5 mm

height of water, which was replaced every day to permit cycles of wetting and drying as well as alkali leaching; (ii) exposure in air to allow alkali leaching and increase CO_2 diffusion of CO_2 into the pore solution (simulating natural carbonation).

Efflorescence was also evaluated by monitoring alkali leaching through the measurement of solution pH. A cylindrical sample of Φ20 × 35 mm (10 ml) was completely immersed in 500 ml of distilled water. The pH of this solution was measured every 10 minutes during the first hour, every hour during the first 6 hours and then daily until 30 days using a Eutech PC 2700 pH and conductivity analyser. To quantify the alkali concentration in the solution surrounding the sample, 10 ml of solution was removed after 30 min, 6 h, 24 h and 28 days and analysed by Shimatzu Atomic Absorption Spectrophotometer (AAS, AA-7000) for the elements Na and K using the emission method. The calibration curve was made using 4 points using distilled water and pure reagents.

Water permeability was quantified using the capillary absorption method where the dried (dried in oven at 50 until mass constancy) cylindrical samples Φ28 × 55 mm were partially immersed in 5 mm of water. This test was performed in a sealed plastic container to prevent water loss and evaporation. The amount of absorbed water was measured every 10 minutes in the first hour and then every hour up to achieve constant mass. The data are reported as the quantity of water absorbed (g) per the cross-sectional area of the sample (cm^2).

Additionally to the water absorption, the pore size distribution was characterised using mercury intrusion porosimetry (MIP) using a Poremaster GT-60 MIP (Quantachrome). Initially the samples were crushed in pieces of about 5 × 5 × 5 mm after 28 d of curing and driet at 60 °C for 4 h. The pore size distribution was determined through the Washburn equation, assuming a surface tension of mercury of 0.485 N/m and a contact angle of 130º. Even though it is widely used, this technique requires some considerations to be applied in the analyses of geopolymers. It should be noted that the high pressure can modify the microstructure of gel and give too high pore volumes. On the same way, MIP consider all the pores as cylindrical and measure the percolated pore volume, not the total pore

volume. However, the technique is widely used for the comparison between different geopolymer systems.

The compressive strength of hardened samples (20 mm cubes) was tested at 28 days of curing using an MTS universal mechanical testing machine with a loading speed of 0.5 mm/min. The density was calculated using the mass and volume of the dried sample used during the water absorption test. The sample was dried in an oven, with 50°C until obtain the mass constancy. The open porosity was calculated from the ratio of the water mass absorbed to the sample volume, using the same samples of water absorption test.

The metakaolin precursor and the geopolymer pastes homogeneity were evaluated using a benchtop scanning electron microscopy (SEM) EVO MA18 40XVP instrument, with a voltage between 10 and 20 kV. The samples were dried at 60 °C for 2 hours and coated with gold during 60s prior to analysis. This equipment is not high resolution but allows the observation of important information related to the materials.

The products formed under the surface of the samples during the partial immersion (treatment i) and carbonation (treatment ii) were analysed at the Brazilian Nanotechnology National Laboratory LNNano (Laboratório Nacional de Nanotecnologia), using a high-resolution FEI Quanta 650 FEG scanning electron microscope (SEM). The instrument was equipped with an Everhart Thomley SED (secondary electron detector) and an In-column detector (ICD) for secondary electrons in bean deceleration (BD) mode. Working with a high resolution Schottky field emission (FEG), accelerating voltage of 10 kV in a probe current ≤ 200 nA. The samples used were a fracture surface of the specimen. Prior to analysis the sample was a dried at 60 °C for 2 hours, placed on a carbon tab and coated with gold for 60 s at a current of 40 A. And a JEOL-JMC-6000PLUS instrument was used to observe the binder after efflorescence, with a voltage of 10 kV.

The samples were analysed by X-ray diffraction (XRD) using a Siemens D5000 diffractometer with Cu Ka radiation (λ=1.54178 Å), with a step size of 0.02°, and a scanning speed of 0.5°/min for a 2θ range of 5 to 70°. Fourier transformed infrared spectroscopy (FTIR) data was acquired using a Perkin

Elmer FTIR spectrometer in absorbance mode from 4000 to 400 cm^{-1}. The data between 600 – 1400 cm^{-1} were deconvoluted using Gaussian curves according to the literature (Rees, et al., 2007).

3. RESULTS AND DISCUSSION

3.1 EFFLORESCENCE FORMATION

3.1.1 Visual inspection

Figure 2 and Figure 3 show the efflorescence formation in the samples after partial immersion in water (treatment i) and environmental conditions (treatment ii), respectively. Figure 2 shows the evolution of efflorescence formation in the system with 20 wt.% of Na_2O cured at room temperature, in ambient conditions, which is also defined as the reference system hereafter. After 28 days of partial immersion in water severe efflorescence formation is identified on the surface of the samples regardless the synthesis conditions (MS content). In particular, after 7 days of partial immersion in water, the system MA 0.0 and MA 0.5 showed higher efflorescence formation when compared to the corresponding systems with MA 1.0. This indicates that addition of soluble silicate in the activator therefore reduces the extent of efflorescence. The differences in extent of efflorescence result from differences in the rate of movement of the alkalis through the pore network in each system, which is controlled by the permeability of the material and the pressure it experiences. The transport process and rate of movement of fluid (in this case alkalis dissolved) obeys Darcy's Law, where the flux ($J=-\kappa.\Delta\rho/\eta$) into the porous material is dependent on permeability (κ), viscosity (η) and pressure (ρ) [32]. The permeability is an intrinsic property of the material and is dependent on the characteristics of the pore network (pore size distribution and tortuosity). On the other hand, pressure is dependent on external conditions. In case of porous materials such as geopolymers, the main pressure which results in movement of fluids is capillary pressure. During evaporation, due to the solid/vapor interface energy, liquid tends to spread from the interior to prevent an increase of pressure [32]. In conditions where evaporation is possible, the drying process allows the movement of fluids to the surface of the geopolymer cement, and consequently results in a high concentration of alkalis on the surface

(typically to the point of saturation). Efflorescence then occurs when the carbonic acid (formed due to partial dissolution of CO_2 in the water) reacts with alkalis in the solution at the surface of the sample to form alkali salts (typically sodium or potassium carbonates) that crystallize and precipitate (defined by humidity and temperature). Efflorescence is therefore dependent on geopolymer microstructural features. The content of soluble silicate in the activator has been shown to control the density (and hence pore size) and therefore plays an important role in retarding efflorescence formation, especially when large quantities of this material (or higher values of MS) are used. These findings are consistent with previous work examining efflorescence in fly ash-based geopolymers [12] and also MK-based geopolymers [21].

Figure 3 also shows a comparison of the evolution of efflorescence formation for all systems where the samples are partially immersed in water (treatment i) and exposed to environmental conditions (treatment ii). The samples with the highest alkali content (Na_2O = 25%) and MS values of 0.5 and 0.0 that were exposed to environmental conditions showed higher efflorescence formation. The systems with higher content of soluble silicate (MS=1.0) did not show any efflorescence formation regardless the alkali concentration (Na_2O = 15, 20 or 25%). This indicates that the addition of soluble silicate in the activator therefore provides higher resistance to efflorescence formation in samples exposed to ambient air. The samples partially immersed in water (treatment i) showed significantly higher efflorescence formation than those exposed to ambient air. Systems in which only Na was used as the alkali source (HA, MA and LA) showed the most severe efflorescence, even at higher values of MS.

A significant reduction in efflorescence formation is identified for systems with 20% of Na+K (i.e. when the alkali source is both Na and K). Among these binary alkali systems (Na+K), the geopolymer with MS = 0.0 showed the highest efflorescence and sample degradation both when partially immersed in water and exposed to ambient air. The system with 20% of Na+K and MS = 0.5 showed a significant reduction in the extent of efflorescence (consistent with the above observation of reduced efflorescence when soluble silicate is added to the activator). However, an unexpected increase in efflorescence was identified for the geopolymer Na+K and MS=1.0. This is consistent with previous

work suggesting that efflorescence formation can be partially prevented by the replacement of Na with K due to the high solubility of potassium carbonate (K_2CO_3)) compared with sodium carbonate ($Na_2CO_3.nH_2O$) [19].

The systems with 20% of Na_2O cured at 50 °C exhibit a reduction in the efflorescence formation compared to those cured at 20 °C, with a reduction of efflorescence again observed with the addition of soluble silicate. This indicates that thermal curing (50 ºC as was assessed here) reduces the susceptibility of geopolymers to efflorescence. This observation is consistent with previous work from [20] and [25], where the reduction was attributed to the pore refinement.

The characteristics of the efflorescence formation differ depending on the geopolymer mix formulation, as shown in Figure 4. In the Figure 4A, a layering process is identified due to extended efflorescence formation in the top of the sample. In the second case (Figure 4B) containing Na and K, the high evaporation and efflorescence growing throughout the sample, which exhibited a low mechanical strength (REF), causing a deeper degradation (~3 mm according to a visual inspection) and higher delayering process. In the last case (Figure 4C) in the geopolymers containing the highest concentration of alkali, a foamier white efflorescence is identified, with delayed degradation (relative to the other samples in this series).

The extent of efflorescence formation is also dependent on the precursors used. In this study with metakaolin as precursor, a larger quantity of alkali activator (between 15-25 wt.% of Na_2O relative to metakaolin mass) was used, much higher than in those studies using pozzolan-based or fly ash precursors which typically use between 5 and 13 wt.% of Na_2O. This behaviour is associated with the reduced amount of amorphous and reactive materials in FA when compared to MK. Thus, the systems under investigation in the current study are therefore more susceptible to efflorescence than work utilising lower amounts of alkali activator.

The molar ratio of Na/Al ranges between 0.67 (Na_2O=15%), 0.88 (Na_2O=20%) and 1.11 (Na_2O=25%), giving nominal values close to or less than the maximum content of Na^+ that can be bound to the gel framework (i.e. such that the molar ratio Al_2O_3/Na_2O=1) when fully reacted [27]. As

the extent of reaction does not progress to 100%, a significant amount of excess alkali (i.e. those not chemically bound to the gel framework) is expected, and will be particularly susceptible to leaching. When lower values are used, the extent of reaction is also lower, inducing less formation of gel, as observer by [21]. Thus, the alkali available to efflorescence formation is derived from the excess of alkali used as activator or from the solubility of this material weakly-bonded, as observed by [21] using a neutral environment (immersion at pH of 7).

In addition to the visible surface efflorescence during carbonation, subflorescence (internal carbonation) is also identified via the carbonate crystals forming inside the pore network closest to the surface (Figure 6). The formation of these products can generate internal stress within the pore network [33,34] and the crystals can sustain a static load on the pore wall, even if the pore expands as a results of cracking [35]. Formation of these crystals in geopolymers can cause significant structural damage [22]. According to Scherer [35], the fracture is not caused by crystalization in a single pore, but the growth of crystals through a region. Thus, during the development of efflorescence, some geopolymer samples exhibited a delayed degradation, which can be attributed to the internal stress resulting from formation of carbonates concentrated in a region of a porous matrix.

The different concentrations of soluble alkalis generate different types of crystals. Figure 5 shows the XRD diffractograms of the superficial efflorescence products scraped from the geopolymer surface in system MA 1.0, MA 0.5 and MA 0.0 (shown in Figure 5A, B, and C, respectively). The results indicate that all the systems are composed of sodium carbonate (Na_2CO_3, Pattern Diffraction File, PDF # 01-086-0301), sodium carbonate monohydrate (thermonatrite, $Na_2CO_3.H_2O$, PDF # 01-070-2148) and sodium carbonate decahydrate (natron, $Na_2CO_3.10H_2O$, PDF # 00-015-0800), aligning with previous observations of efflorescence products in geopolymers produced with fly ash [12,19,36]. A broad feature centred at 22 degrees 2θ is also observed and attributed to the presence a small amount of amorphous geopolymer gel. The extent of hydration of sodium carbonate is dependent on the content of alkali concentration, temperature, humidity, and capillary pressure. Crystallization of sodium carbonate decahydrate occurs at low concentration in the pore solution, initiating near to 0.6 Na_2CO_3 mol/l at 0 °C to 4.3 Na_2CO_3 mol/l at 32 °C [37–39]. The increasing of this temperature

induces the formation of monohydrates ($Na_2CO_3.H_2O$) and anhydrous (Na_2CO_3) phases [37–39]. In the current study, systems with lower amounts of soluble silicate in the activator exhibit higher intensity reflections in the diffractograms, indicating that lower amounts of soluble silicate in the activator results in formation of a higher amount of sodium carbonate phases. According to previous works [22,33] the amount of sodium carbonate phase formation is controlled by the crystallization pressure and humidity within the pore network, while the extent of carbonation and pore size controls the deterioration of the geopolymers cement. These statements are consistent with that observed here, where the extent of efflorescence is dependent on the properties of the formed gel. This is also coherent with the decreased levels of efflorescence and sample deterioration with increased amounts of soluble silicate in the activator.

In addition to acquisition of XRD data, sections of the degraded samples (exclusively from the Na_2O 20% system) were analyzed by SEM (Figure 6 A, B and C) to observe their morphology. For comparison, drops of each activator solution was dried under controlled condtions (temperature of 20 ± 5 °C and RH of 65 ± 20%) in order to promotes their alkali salt crystallization (in the absence of the geopolymer cement or metakolin precursor). These crystals were also analysed by SEM as shown in in Figure 6 D, E, and F.

Figure 6A (geopolymer) and Figure 6D (crystallised activator) correspond to the system MA 1.0 with high amounts of soluble silicate. The crystals formed on the geopolymer surface (Figure 6A) are small crystals (< 10 μm). Figure 6D shows bigger crystals formed after crystallisation of the activator in contact with air, where layers of crystals in different directions can be observed. The formation of larger crystals is observed on the surface of the geopolymer and the crystallised activator for the system MA 0.5 with moderate amounts of soluble silicate, as shown in Figure 6B and Figure 6E. The geopolymer and crystallized activator for the system MA 0.0 without soluble silicate in Fig 6C and Figure 6F show the formation of the largest crystals in the form of both needles and platelets (> 20 μm) . These largest crystals propably explainthe higher degree of degradation identified for the NaOH-based geopolymers (MS=0.0). Both the geopolymer and crystallised activator that do not contain soluble silicate exhibit a different morphology when compared to the crystallised activator

containing soluble silicate, showing the formation of needle-like crystals rather than plate-like crystals. The crystal formation is associated with the amount of leached material and its composition, where the different shapes and sizes of the crystals indicate the formation of different products.

3.1.2 Evaluation of efflorescence potential using pH measurement

As efflorescence formation results from movement of free alkalis to the surface, the susceptibility of geopolymers to efflorescence can be quantified by measuring the pH of the solution in contact with the sample. The pH analysis of the solutions in which geopolymer samples were fully immersed in water for up to 600 hours are shown in Figure 7. Each solution exhibited a rapid rise in the pH, with a value of ~10.5 being reached after only 2 minutes, and a value of 11 – 11.5 being reached after 2 hours of immersion. In all systems, geopolymers with high amounts of soluble silicate (MS = 1.0) exhibit lower pH values than those prepared with lower amounts (MS = 0.5) or without sodium silicate (MS = 0.0). This is consistent with the visual appearance of the samples (Figure 3), where the efflorescence formation takes a longer time for geopolymers with MS = 1.0. The values measured also showed a direct relation between pH and alkali concentration in the activator, where highest alkalinity in the solution was identified for the samples activated at 25% of Na_2O. Therefore, higher alkali leaching rates were observed in samples with higher alkali content in the activator. Increased amounts of soluble silicate in the activator in mixed alkali systems ($Na^+ + K^+$) reduces the pH values of the solution assessed when compared to those where the only alkali source was Na^+ (consistent with the visual observations of efflorescence in Figure 3). The systems with thermal curing (50 °C for the first 24 hours, then 20 °C thereafter) also exhibit lower pH values when compared to the corresponding systems cured at 20 °C, in agreement with visual observations of efflorescence (Figure 3). In general, the results show increasing pH values (and therefore alkali leaching) over time for all samples assessed. Previous work has reported pH values between 11 and 12 up to 3 days of analysis using fly ash as precursor and the amount of alkalis (represented by the percentage in mass of alkalis relative to precursor) between 5.8 and 6.5 wt.% when 1.2-1.5 mm particles sizes are tested [12]. The values observed in the study are higher due to the increased alkali content in the activator (between 3 and 4 times higher), longer exposure time and smaller particle sizes.

3.1.3 Evaluation of efflorescence potential by alkali leaching analysis

In addition to the measurement of pH, the concentrations of Na^+ and K^+ in solutions from the leaching experiments were quantified using AAS (Figure 8). The analysis was performed according to the type of alkali used as the activator (Na, K or Na + K). The increasing in the use of soluble silicate results in lower alkali concentration in solution (and hence lower alkali leaching), and is particularly evident during the early stages of leaching. On average, the addition of sodium silicate (MS = 1.0) provides a reduction of approximately 14% when compared to hydroxide-based systems. This is consistent with the pH values discussed above and is attributed to the stronger chemical bonding of the alkalis to the gel framework, the greater sample density (consistent with the higher compressive strength) and pore network tortuosity in geopolymers with MS > 0.0. The reduction in alkalis leached from the geopolymer with increasing soluble silicate in the activator is also observed in mixed alkali (Na^+ + K^+) systems. However, in the absence of soluble silicates mixed alkali systems (Na+K 0.0) showed higher alkali leaching. This is attributed to a lower extent of reaction and geopolymer formation observed in these samples (Longhi et al., (2019b)), where the use of KOH as the main alkali activator results in lower precursor dissolution and gel formation. Minimal efflorescence formation was observed visually in these mixed alkali systems (Figure 3), even with high alkali concentrations. According to Škvára *et al*., (2009), K_2CO_3 presents a high solubility when compared with Na_2CO_3 at 20°C, which results in lower precipitation of K_2CO_3 crystals and hence a lower extent of visible efflorescence. According to Zeng and Zheng [40], the solubility of the salt K_2CO_3 (112g/l at 20°C) is much higher than Na_2CO_3 (30g/l at 20°C) and generates a smaller crystallization area. Thermal curing reduces alkali leaching effectively (with a final Na^+ concentration of 220 ppm after 28 days). This is ~9% lower than the alkalis leached in the reference system (with a final Na^+ concentration of 240 ppm after 28 days). Therefore, higher levels of soluble silicate and hydrothermal treatment are the most effective synthesis parameters to reduce leaching.

For the MK-based geopolymers assessed in this work, a dissolved alkali concentration of between 197.6 ppm (cured at 50 °C and MS of 1.0) and 392.7 ppm (Na+K 0.0) was observed, corresponding to 17% and 30% of the original alkali concentration used in the activator. Zhang et al. [20] reported a

concentration of 12% and 16% of sodium and potassium, respectively, in fly ash-based geopolymers after 24 hours of immersion in water (concentrations of around 100 to 150 ppm). This difference is believed due to the differences of sample size and reaction product. Another previous study published by Zheng *et al*. [41] found a leaching ratio between 40 and 60% of the original sodium from cylindrical fly ash-based geopolymer after immersion in a nitric acidic solution with pH adjusted to 4 during 45 h. That is attributed the high leaching levels to the low reactivity of the precursor and the replacement of Na^+ by H^+.

Based on the results shown previously, the pH and alkali concentration measurements indicate that the extent of alkali leaching is directly controlled by the geopolymer mix proportioning, as these determine the amount of free alkalis within the geopolymer cement. The addition of sodium silicate as part of the activator is found to be the primary synthesis parameter that can be used to reduce the content of free alkalis, increase sample density and pore network tortuosity (as will be shown below), and hence susceptibility to efflorescence and subsequent material degradation.

3.2 PHYSICAL PROPERTIES

The physical properties of geopolymer cements are important to predict their behaviour during service life. According to previous studies, the porosity and pore structure significantly affect the extent of efflorescence formation, as lower permeability results in a reduction in alkali leaching and internal carbonation [12].

3.2.1 Capillarity water absorption

The water absorption of each sample by capillarity is shown in Figure 9. In the systems with less amount of sodium silicate, the mass increased progressively up to 24 hours, and then remained unchanged beyond this point, indicating the saturation point. Regardless the alkali concentration (15% to 25% of Na_2O), the absorption of water is significantly reduced (mainly during the first hours) in samples where the activator higher amounts of soluble silicate (MS = 1.0). The MA 1.0 and HA 1.0 geopolymers showed the lowest water permeability with values of approximately 2 g/cm². The use of mixed alkali (Na^+ + K^+) as part of the activator provided a slower absorption at the beginning of the

measurements, but after 24 h the Na+K 1.0 geopolymer showed up to 25% higher values when compared to the corresponding Na-based systems. Thermal curing showed the same behaviour when compared to the reference system, and final water absorption is slightly higher. The trends of water absorption correlate directly with the pH measurements, extent of alkali leaching and visual observation of efflorescence. Therefore, is clear that the degree of water permeability also plays an important role in the extent of alkali leaching and hence efflorescence in these systems.

3.2.2 Density and total porosity

The density and total porosity of each sample, measured by water absorption, are shown in Figure 10, while the compressive strength of each sample is presented in Table 1. Summarising the compressive strength data, the higher values were obtained in systems with greater Na_2O content. This is because increased Na_2O content results in an increased activator pH, which drives increased precursor dissolution and consequently greater gel formation. Also, the addition of soluble silicate induces the formation of a microstructure with more tetrahedral bounded Si in $Q^4(1Al)$ and $Q^4(2Al)$ coordination, providing a stronger material [21]. The use of potassium as part of the activator significantly decreased the compressive strength by ~50%, and particularly for samples containing low amounts of soluble silicates and samples that experienced thermal curing.

As expected, higher density is aligned to higher compressive strength. A higher density was identified in systems with medium sodium content in the activator (20%) and is reduced with lower sodium content or the presence of potassium in the activator. The porosity presented in Figure 10 represents the void volume or open porosity in relation to the volume of the sample. The behaviour is also consistent with the other analyses and confirms a lower porosity is observed in denser and stronger systems. The values observed here are higher than those published by Zhang *et al.* [22], where the open porosity of fly ash geopolymers was between 17 and 45%. This is consistent with the higher rate of water absorption and higher alkali leaching observed in metakaolin-based geopolymers when compared to fly ash-based geopolymers.

Figure 11 shows the pore size fractions and mean pore size determined by MIP, which are generally lower than those determined by water absorption. The dimensional limit of MIP in this analysis is 5.5 nm, and smaller pores than this are not able to be quantified. Additionally, MIP can only measure the total accessible or percolated pore volume and not the total pore volume (i.e. including those not connected to the sample surface [42]. Thus, the difference observed between water absorption and MIP can be attributed those pores that are not connected and those with diameter size smaller than 5.5 nm.

The mean pore size defined from MIP data indicates that using higher content of alkali and soluble silicates in the activator results in the formation of smaller pore, consistent with the density values (Figure 10). The effect of a larger pore size distribution lead to the reduction of compressive strength values. These values corroborate the high permeability and subsequent higher susceptibility to alkali leaching, which is also coherent with the results presented in Figure 9.

The relation between physical properties and efflorescence formation is also important. The systems with 25% of Na_2O presented the higher compressive strength, however, in all systems, the efflorescence formation was observed only in the samples exposed to air condition (treatment ii). This indicates an excess of alkalis in these systems. The use of potassium within the activator decreased the compressive strength but also reduced the visual efflorescence formation. Therefore, even though the compressive strength is directly related to density and porosity but it cannot be used as an index for efflorescence formation. In this sense, the porosity and water absorption are the main parameters that plays a significant role in the susceptibility for efflorescence development. These relations between leaching potential and physical properties show that it is possible to reduce the leaching process if a denser geopolymer material is synthesized.

The morphologies of selected geopolymer samples after 28 days (without exposure treatments i or ii) were also assessed using SEM (Figure 12). The homogeneity of the material indicates the large extent of reaction between the activator and the precursor. In a system with a lower reaction degree, the matrix looks less compact and unreacted MK particles can be observed, which is consistent with what

was previously observed by Longhi et. al [21]. In the geopolymer HA 1.0 (Figure 12A) the formation of a strong and dense matrix is visible, without any unreacted MK particles. The geopolymers MA 1.0 (Figure 12B) and LA 1.0 (Figure 12C) also shows a homogeneous and dense structure, but with the presence of more free unreacted MK particles (lighter grey particles in the images). The geopolymers MA 0.5 (Figure 12D) and MA 0.0 (Figure 12E) show increased amounts of unreacted MK particles and a less compact structure compared with the MA 1.0 system, which agrees with its lower density and less extent of reaction with a reduction of soluble silicates in the activator, as observed previously [21]. This is also consistent with the lower mechanical performance and higher water absorption in these samples, as discussed above.

3.3 MICROSTRUCTURAL PROPERTIES

A detailed analysis of geopolymer microstructure and its relation to mechanical and chemical properties was performed, and correlated with the efflorescence formation to elucidate the underlying mechanisms of efflorescence formation.

3.3.1 XRD

The X-ray diffractograms of the geopolymer and the unreacted MK precursor are shown in Figure 13. The metakaolin exhibits the formation of a broad feature due to diffuse scattering between 15 and 35° 2θ, indicating the predominant amorphous nature. Crystalline phases such as anatase (TiO_2, Pattern Diffraction File, PDF# 00-021-1272) and halloysite ($Al_2Si_2O_5(OH)_4$, PDF #00-029-1489) are also identified. After alkali activation, a broad feature due to diffuse scattering is observed at approximately 30° 2θ and is attributed to formation of an alkali aluminosilicate (geopolymer) gel framework. Reflections due to anatase are also observed in the XRD data for the geopolymer samples, indicating that this phase is largely inert during alkali activation. Reflections due to zeolite A ($Na_{96}Al_{96}Si_{96}O_{384}\cdot 216H_2O$; PDF# 00-039-0272) are also observed in the hydroxide-based geopolymer systems, and the formation of this phase is enhanced in systems with thermal curing and containing higher amounts of alkali in the activator (HA 0.0). Formation of zeolites in geopolymers is relatively common, due to their pseudo-zeolitic structure, and zeolite A has been previously reported as a

reacted product formed in MK-based geopolymers with hydroxide as the activator [43]. The XRD characterization of geopolymer cannot define the extend of efflorescence formation, however, is an important analysis to identify the products formed and their possible influence on the phenomenon formation.

3.3.2 FTIR

The results of the FTIR spectra of geopolymers systems without exposition to the efflorescence process are shown in Figure 14. The metakaolin exhibits a main peak around 1080 cm^{-1}, attributed to the asymmetric stretching vibration of Si-O-T (T=Si or Al) [44]. The second broad peak in the bands around 800 cm^{-1} is attributed to the Al-O bending of AlO_6 octahedral sites within metakaolin [43]. After alkali activation, all systems exhibit a main peak between 900 and 1000 cm^{-1} that is attributed to the asymmetric stretching vibration mode of Si-O-T bonds, characteristic of geopolymer gel formation [45]. The peak between 660 and 730cm^{-1} represents the O-Si-O band, corresponding to quartz or zeolite species [45]. The peak near to 1400 cm^{-1} can be attributed to asymmetric stretching of the O-C-O bond, and related to the sample carbonation [43], however, this carbonation occurs during sample preparation and is not related to the efflorescence induced by the different treatments. The peaks near to 1650 cm^{-1} are attributed to the surface hydroxyl groups hydrogen-bonded to the adsorbed water [43,46].

Figure 15 shows the FTIR spectra and associated deconvolutions between 1300 and 500 cm^{-1}. The spectrum was fit manually with the minimum number of peaks, with the requirement of a fitting coefficient higher than 0.99. The activated at 20% of Na_2O shows five peaks, with some differences according to the addition of soluble silicate (or MS value used during the synthesis). The two main peaks are between 1041 - 1009 cm^{-1} and 971 - 955 cm^{-1}. The band between 1020 - 998 cm^{-1} is assigned to asymmetric stretching vibrations of Si-O-T [31,43,45] and the band at 940 - 979 cm^{-1} to asymmetric stretching vibrations of non-bridging oxygen sites, in this case Si-O-Na [31,43]. The addition of sodium silicate (MS> 0.0) promotes the shift of these bands to higher wavenumbers, due to the addition of soluble silicate and provides a higher amount of Si in the vibration associated with Si-O-T, consistent with other studies [31]. Likewise, the characteristic vibration of Si-O-Na, indicated

more content of bounded Na by the addition of extra Si. This microstructural change has a strong effect on the mechanical properties of geopolymers and the alkali leaching potential (Figure 7 and Figure 8). Thus, better performance is observed from the addition of soluble silicates and indicates a more resistant structure in the presence of greater quantities of Si bounded to the structure. The bands near to 859 cm^{-1}, can be associated to the bending in the Si-OH group [31] and the peak near to 690 cm^{-1} represents the bending of Al-O-Si bonds [47].

Regardless of the activator composition, the deconvoluted FTIR spectra are generally similar. The main difference is related to the peak near to 855 cm^{-1}, characteristic of bending in Si-OH group and associated with the soluble silicate content used as activator. More amount of Na_2O indicates more Si-OH bonds, which indicates the excess hydroxyl groups provided by the activator. The spectra for the system with medium alkali with and without thermal curing do not show significant differences, which is consistent with the other analyses discussed above. The geopolymers synthetized with KOH as part of the activator shows different bands in the FTIR spectra. The use of high content of sodium silicate provides a spectrum similar to the "Na system"; however, the addition of more potassium in the mixture generates the formation of a new peak near to 1100 cm^{-1} and the shift of other peaks. The new peak located at 1126 cm^{-1} can be attributed to the formation of Si-O-K bound, where the intensity is relative to the quantity of KOH used. A reduction of Si-O-Na bonds is also observed, consistent with the synthesis parameters.

The FTIR analysis shows that the structure type formed is closely related to efflorescence formation. A greater amount of Si-O-T bonds indicate the formation of a denser and stronger material, with less water absorption and consequently lower alkali movement. The addition of soluble silicates results in increased incorporation of alkalis into the framework structure of the gel, which reduces the leaching potential. These results are in agreement with the alkali leaching content and visual efflorescence formation.

4. CONCLUSIONS

Overall, this work shows that efflorescence formation is dependent on chemical and physical properties of geopolymer cements, particularly the amount of free alkalis, density, porosity and water absorption. As properties are controlled by the physicochemical characteristics of the precursor and the alkali activator type and content, efflorescence formation is totally dependent on the mix proportioning parameters (primarily the alkalis content and presence of soluble silicates).

Increased soluble silicate in the activator results in lower efflorescence formation. This reduction is associated with the higher amount of Si in the geopolymer gel, reducing such as porosity and permeability and retarding the leaching process. Similarly, increasing of alkali dosage provides a strong material due to the greater reaction extent. However, a higher amount of alkalis can induce the higher amount of free alkalis, so there exists an optimum point at which minimum efflorescence can be achieved.

The cation present in the alkaline activator influences extent of efflorescence formation and mechanical behaviour. The use of potassium as the alkali source results in an apparent reduction of efflorescence when observed visually, but also reduces the density and mechanical strength of the material. The apparent reduction of efflorescence formation in potassium based-geopolymers is in fact due to high solubility of the carbonate formed.

The use of thermal curing (50 °C) looks effective for a specific sample which is consistent to the reduction of alkali leached, however, in the other nanostructural and physical analysis, the behaviour is similar when compared to the geopolymers cured at ambient temperature. Due to the high reactivity of the metakaolin used and the high amount of activator, the improvement of properties using additional temperature is less expressive when compared to its use in low reactivity precursors.

Thus, although every geopolymer will contain some extent of free and leachable alkalis, the amount of alkalis in the framework structure of the gel can be optimised by careful control of the synthesis parameters. This reduces permeability and increases the tortuosity of the pore network, consequently retarding the movement of free alkalis and lowering efflorescence formation. The effect of

efflorescence on the durability and mechanical properties of geopolymers remains unclear, and presents an important line of future investigation.

ACKNOWLEDGEMENTS

Funding from Australian Research Council through a Discovery project and a DECRA DE/170/101070 project. The participation of Brazilian authors was sponsored by CNPq (Brazilian National Council for Scientific and Technological Development) through the research project UNIVERSAL grant number 458597/2014-7, as well as the research fellowships PQ2017 303753/2017-0 and 305530/2017-8. M.A. Longhi is grateful for the financial support of CAPES and of SWE 203750/2017-9. The participation of B. Walkley was supported by the Engineering and Physical Sciences Research Council (UK) through grant EP/P013171/1.

REFERENCES:

[1] Glasby T, Day J, Genrich R, Aldred J. EFC geopolymer concrete aircraft pavements at Brisbane West Wellcamp Airport. Concr Conf 2015;11:1–9. https://www.geopolymer.org/fichiers_pdf/GP-AIRPORT.pdf..

[2] Passuello A, Rodríguez ED, Hirt E, Longhi MA, Bernal SA, Provis JL, Kirchheim AP. Evaluation of the potential improvement in the environmental footprint of geopolymers using waste-derived activators. J Clean Prod 2017; 166:680–689. https://doi.org/10.1016/j.jclepro.2017.08.007.

[3] Van Deventer JSJ, Provis JL, Duxson P. Technical and commercial progress in the adoption of geopolymer cement. Miner Eng 2012;29:89–104. https://doi.org/10.1016/j.mineng.2011.09.009.

[4] Duxson P, Van Deventer JSJ. Commercialization of geopolymers for construction – opportunities and obstacles. In: Provis JL, van Deventer JS. Geopolymers, Woodhead Publishing, 2009: pp. 379–400. https://doi.org/10.1533/9781845696382.3.379.

[5] Duxson P, Provis JL, Lukey GC, van Deventer JSJ. The role of inorganic polymer technology in the development of 'green concrete'. Cem Concr Res. 2007;37:1590–1597. https://doi.org/10.1016/j.cemconres.2007.08.018.

[6] Provis JL. Geopolymers and other alkali activated materials: why, how, and what?, Mater Struct 2013;47:11–25. https://doi.org/10.1617/s11527-013-0211-5.

[7] Bernal S, Rodríguez E, Kircheiim AP, Provis J. Management and valorisation of wastes through use in producing alkali-activated cementmaterials, J Chem Technol Biotechnol 2016;91:2365–2388. https://doi.org/10.1002/jctb.4927.

[8] Habert G, d'Espinose de Lacaillerie JB, Roussel N. An environmental evaluation of geopolymer based concrete production: reviewing current research trends. J Clean Prod 2011;19:1229–1238. https://doi.org/10.1016/j.jclepro.2011.03.012

[9] Heath A, Paine K, McManus M. Minimising the global warming potential of clay based geopolymers. J Clean Prod 2014;78:75–83. https://doi.org/10.1016/j.jclepro.2014.04.046.

[10] Habert G, Ouellet-plamondon C. Recent update on the environmental impact of geopolymers. Rilem Tech Lett 1 2016;17–23. https://doi.org/10.21809/rilemtechlett.2016.6.

[11] Zhang Z, Yao X, Zhu H. Potential application of geopolymers as protection coatings for marine concrete II. microstructure and anticorrosion mechanism. Appl Clay Sci 2010;49:7–12. https://doi.org/10.1016/j.clay.2010.04.024.

[12] Zhang Z, Provis JL, Reid A, Wang H. Fly ash-based geopolymers: The relationship between composition, pore structure and efflorescence. Cem Concr Res 2014;64:30–41. https://doi.org/10.1016/j.cemconres.2014.06.004.

[13] Bakharev T. Durability of geopolymer materials in sodium and magnesium sulfate solutions. Cem Concr Res 2005:35;1233–1246. https://doi.org/10.1016/j.cemconres. 2004.09.002.

[14] Fernandez-Jimenez A, Palomo A. Nanostructure/microstructure of fly ash geopolymers. In: Provis JL, van Deventer JSJ, editors. Geopolymers, Woodhead Publishing, 2009: pp. 89–117.

[15] Bernal SA, Provis JL. Durability of alkali-activated materials: Progress and perspectives. J Am

Ceram Soc 2014;97:997–1008. https://doi.org/10.1111/jace.12831..

[16] Provis JL, Van Deventer JSJ. Alkali Activated Materials State of the Art Report. RILEM TC 224-AAM, 2014. https://doi.org/10.1007/978-94-007-7672-2

[17] Provis JL, Bernal SA. Geopolymers and Related Alkali-Activated Materials. Annu Rev Mater Res 2 2014;44:3.1-3.29.https://doi:10.1146/annurev-matsci-070813-113515.

[18] Longhi MA, Zhang Z, Rodríguez ED, Kirchheim AP. Efflorescence of Alkali-Activated Cements (Geopolymers) and the Impacts on Material Structures: A Critical Analysis. Frontiers in Materials 2019;6:1–13. https://doi.org/10.3389/fmats.2019.00089.

[19] Škvára F, Kopecký L, Myšková L, Šmilauer VÍT, Alberovská L, Vinšová L. Aluminosilicate polymers - Influence of elevated temperatures, efflorescence, Ceram - Silikaty 2009;53:276–282.

[20] Zhang Z, Provis JL, Reid A, Wang H. Fly ash-based geopolymers: The relationship between composition, pore structure and efflorescence. Cem Concr Res 2014;64:30–41. https://doi.org/10.1016/j.cemconres.2014.06.004.

[21] Longhi MA, Walkley B, Rodríguez ED, Kirchheim AP, Zhang Z, Wang H. New selective dissolution process to quantify reaction extent and product stability in metakaolin-based geopolymers. Compos Part B Eng 2019;176:107172. https://doi.org/10.1016/j.compositesb.2019.107172.

[22] Zhang Z, Provis JL, Ma X, Reid A, Wang H. Efflorescence and subflorescence induced microstructural and mechanical evolution in fly ash-based geopolymers. Cem Concr Compos 2018;92:165–177. https://doi.org/10.1016/j.cemconcomp.2018.06.010.

[23] Dow C, Glasser FP. Calcium carbonate efflorescence on Portland cement and building materials. Cem Concr Res 2003;33:147–154. https://doi.org/10.1016/S0008-8846(02)00937-7.

[24] Škvára F, Šmilauer V, Hlaváček P, Kopecký L, Cílová Z. A weak alkali bond in (N, K)-A-S-H gels: Evidence from leaching and modeling, Ceram - Silikaty. 2012;56:374–382.

[25] Najafi E, Allahverdi A, Provis JL. Efflorescence control in geopolymer binders based on natural pozzolan. Cem Concr Comp. 2012;34:25–33. https://doi.org/10.1016/j.cemconcomp.2011.07.007.

[26] Yao X, Yang T, Zhang Z. Compressive strength development and shrinkage of alkali-activated fly ash–slag blends associated with efflorescence. Mater Struct Constr 2016;49:2907–2918. https://doi.org/10.1617/s11527-015-0694-3.

[27] Fernández-Jiménez a., Palomo a., Sobrados I, Sanz J. The role played by the reactive alumina content in the alkaline activation of fly ashes. Micro Meso Mater 2006;91:111–119. https://doi.org/10.1016/j.micromeso.2005.11.015.

[28] Walkley B, Rees GJ, Nicolas RS, Deventer JSJ Van, Hanna J V, Provis JL. New Structural Model of Hydrous Sodium Aluminosilicate Gels and the Role of Charge-Balancing Extra-Framework Al. Phys Chem 2018;122:5673-5685. https://doi.org/10.1021/acs.jpcc.8b00259.

[29] Duxson P, Lukey GC, Separovic F, van Deventer JSJ. Effect of alkali cations on aluminum incorporation in geopolymeric gels. Ind Eng Chem Res 2005;44:832–839. https://doi.org/10.1021/ie0494216.

[30] Longhi MA, Rodríguez ED, Bernal SA, Provis JL, Kirchheim AP. Valorisation of a kaolin

mining waste for the production of geopolymers. J Clean Prod 2006;115:265-272. https://doi.org/10.1016/j.jclepro.2015.12.011.

[31] Zhang Z, Provis JL, Wang H, Bullen F, Reid A. Quantitative kinetic and structural analysis of geopolymers. Part 2. Thermodynamics of sodium silicate activation of metakaolin. Thermochim Acta 2013;565:163–171. https://doi.org/10.1016/j.tca.2013.01.040.

[32] Scherer GW. Theory of Drying. J Am Chem Soc 199;14:3-14. https://doi.org/10.1111/j.1151-2916.1990.tb05082.x

[33] Scherer GW. Stress from crystallization of salt. Cem Concr Res 2004;34:1613–1624. https://doi.org/10.1016/j.cemconres.2003.12.034.

[34] Desarnaud J, Bonn D, Shahidzadeh N. The Pressure induced by salt crystallization in confinement. Sci Rep 2016;6:23–26. https://doi.org/10.1038/srep30856.

[35] Scherer GW. Crystallization in pores. Cem Concr Res 1999;29:1347–1358. https://doi.org/10.1016/S0008-8846(99)00002-2

[36] Burciaga-Díaz O, Escalante-García JI, Arellano-Aguilar R, Gorokhovsky Statistical analysis of strength development as a function of various parameters on activated metakaolin/slag cements. J Am Ceram Soc 2010;93:541–547. https://doi.org/10.1111/j.1551-2916.2009.03414.x.

[37] Wells RC, McAdam DJ. Phase relations of the system: Sodium carbonate and water. J Am Chem Soc 1907;29:721–727. https://doi.org/10.1021/ja01959a009.

[38] Kobe K, Sheehy T. Addendum. Thermochemistry of Sodium Carbonate and It's Solutions. Ind Eng Chem 1948;40;2370–2370. https://doi.org/10.1021/ie50468a600.

[39] Mahmoudkhani M, Keith DW. Low-energy sodium hydroxide recovery for CO_2 capture from atmospheric air-Thermodynamic analysis. Int J Greenh Gas Control 2009;3:376–384. https://doi.org/10.1016/j.ijggc.2009.02.003.

[40] Zeng Y, Zheng Z. Phase Equilibria for the Aqueous System Containing Sodium, Potassium, Carbonate, and Sulfate Ions at 273.15 K. J Chem Eng Data 2009:1244–1248. https://doi.org/10.1021/je800641k.

[41] Zheng L, Wang C, Wang W, Shi Y, Gao X. Immobilization of MSWI fly ash through geopolymerization: Effects of water-wash, Waste Manag. 2011;31:311–317. https://doi.org/10.1016/j.wasman.2010.05.015.

[42] Scrivener K, Snellings R, Lothenbach B. A Practical Guide to Microstructural Analysis of Cementitious Materials - Chapter 5: Thermogravimetrix Analysis. Taylon and. Boca Raton: CRC press; 2016.

[43] Zhang Z, Wang H, Provis JL, Bullen F, Reid A, Zhu Y. Quantitative kinetic and structural analysis of geopolymers. Part 1. The activation of metakaolin with sodium hydroxide, Thermochim. Acta. 2012;539:23–33. https://doi.org/10.1016/j.tca.2012.03.021.

[44] Rees CA, Provis JL, Lukey GC, Deventer JSJ Van. Attenuated Total Reflectance Fourier Transform Infrared Analysis of Fly Ash Geopolymer Gel Aging. Langmuir. 2007;23:8170–8179. https://doi.org/10.1021/la700713g

[45] Criado M, Palomo A, Fernandez-Jimenez A. Alkali activation of fly ashes. Part 1: Effect of curing conditions on the carbonation of the reaction products. Fuel 2005;84:2048–2054.

https://doi.org/10.1016/j.fuel.2005.03.030.

[46] Giannopoulou I, Panias D. Hydrolytic stability of sodium silicate gels in the presence of aluminum. J Mater Sci 2010;45:5370–5377. https://doi.org/10.1007/s10853-010-4586-1.

[47] Bernal SA., Provis JL, Rose V, Mejía de Gutierrez R. Evolution of binder structure in sodium silicate-activated slag-metakaolin blends. Cem Concr Compos 2011;33:46–54. https://doi.org/10.1016/j.cemconcomp.2010.09.004.

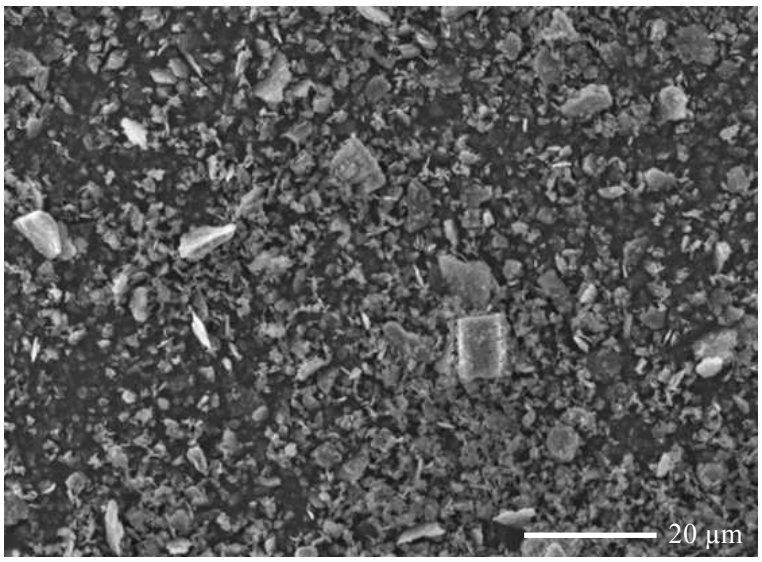

Figure 1– Scanning Electron Microscope (SEM) secondary electron image of the commercial metakaolin used in this study.

Table 1 - Proportion of geopolymer samples and the compressive strength at 28-days.

Geopolymers	Design parameters				Compressive strength (MPa)	Standard deviation (MPa)
	wt. % M_2O	MS modulus	Alkali	Temperature (°C)		
HA 0.0	25	0	Na	25	20.00	1.8
HA 0.5	25	0.5	Na	25	23.50	1.1
HA 1.0	25	1	Na	25	44.97	5.3
MA 0.0	20	0	Na	25	10.45	1.1
MA 0.5	20	0.5	Na	25	23.75	1.5
MA 1.0	20	1	Na	25	40.13	2.9
LA 0.0	15	0	Na	25	6.59	0.5
LA 0.5	15	0.5	Na	25	7.84	0.6
LA 1.0	15	1	Na	25	21.52	2.4
Na+K 0.0	20	0	Na+K	25	0.83	0.1
Na+K 0.5	20	0.5	Na+K	25	7.29	0.5
Na+K 1.0	20	1	Na+K	25	30.2	3.6
50°C 0.0	20	0	Na	50	13.92	1.3
50°C 0.5	20	0.5	Na	50	19.18	2.2
50°C 1.0	20	1	Na	50	35.15	3.2

HA=25% Na_2O, **MA**=20% Na_2O, **LA**=15% Na_2O, **Na+K**=20%Na_2O+K_2O, **50°C**= 20% Na_2O + curing at 50°C

M_2O= Na_2O + K_2O, **MS modulus=** SiO_2/M_2O molar ratio

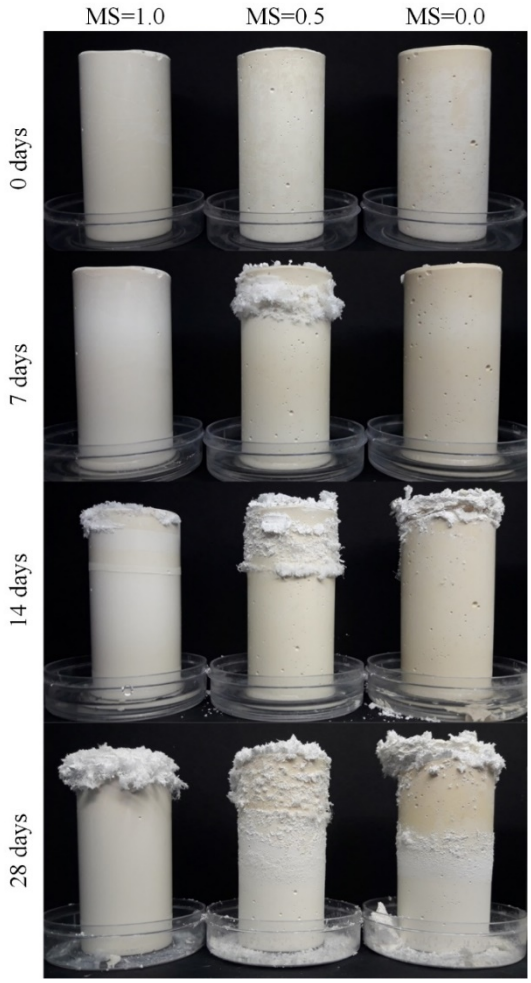

Figure 2 – Images of the evolution of efflorescence during 28 days for the systems with 20% of Na_2O and different contents of soluble silicate in the activator (MS = 0, 0.5, and 1.0). All samples were partially immersed in water as described in the text.

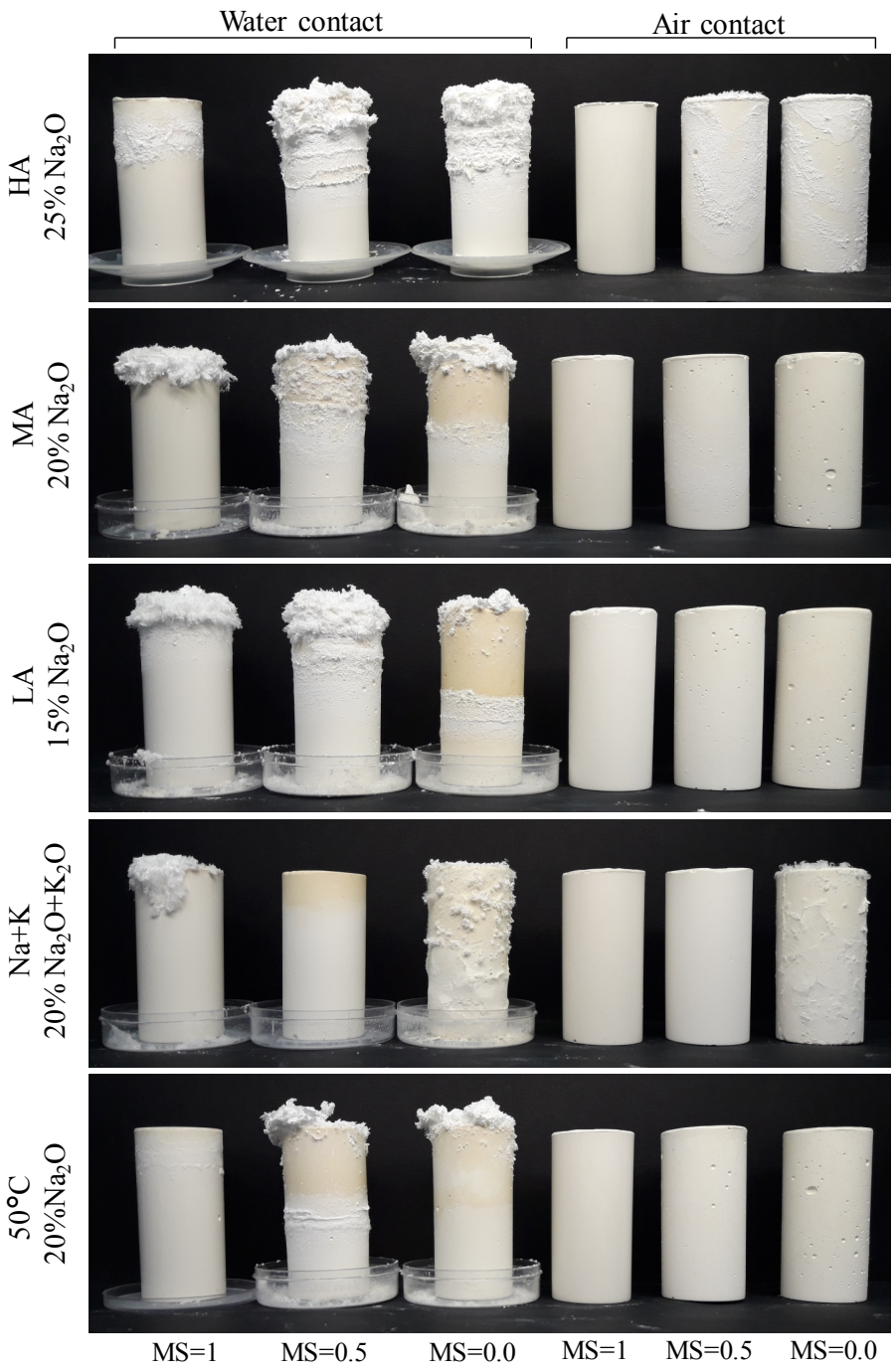

Figure 3 – Images of efflorescence of geopolymer samples after 28 days of either partial immersion in water and exposure to environmental conditions (air contact) **HA**= 25% Na_2O, **MA**= 20% Na_2O, **LA**= 15% Na_2O, **Na+K**=20% Na_2O+K_2O, **50°C**= 20% Na_2O + curing at 50°C.

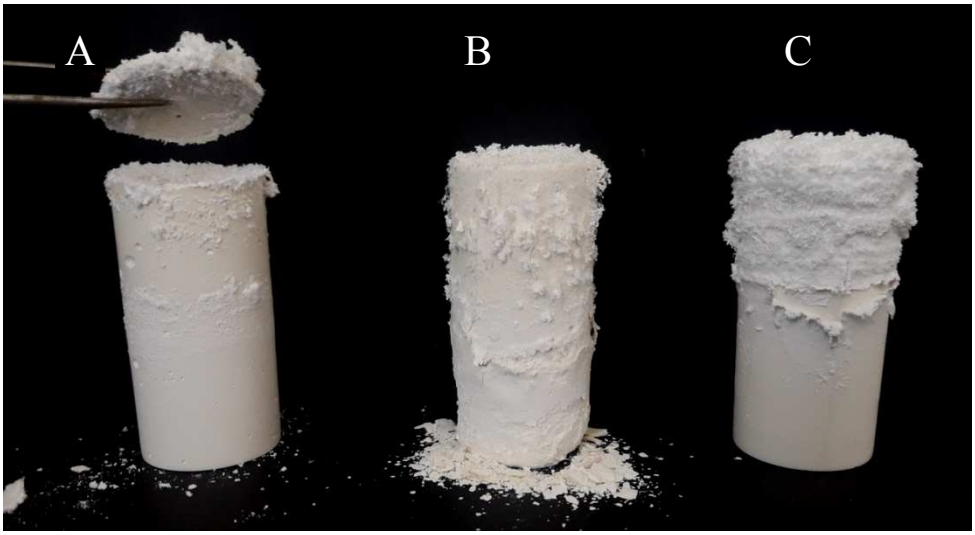

Figure 4 - Highest attack/deterioration by the effloresecnece formation in NaOH-based geopolymer samples: A. MA 0.0, B. Na+K 0.0 and C. HA 0.0

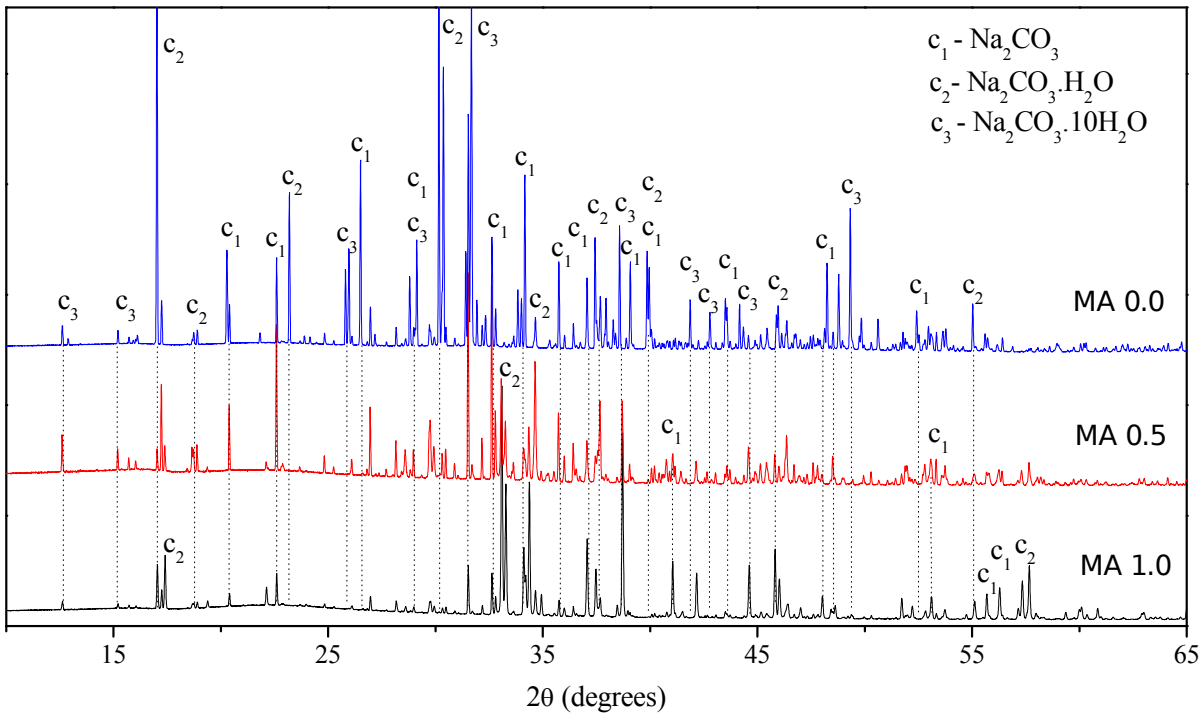

Figure 5 – XRD patterns of the efflorescence products from the surface of geopolymers MA 1.0, MA 0.5 and MA 0.0.

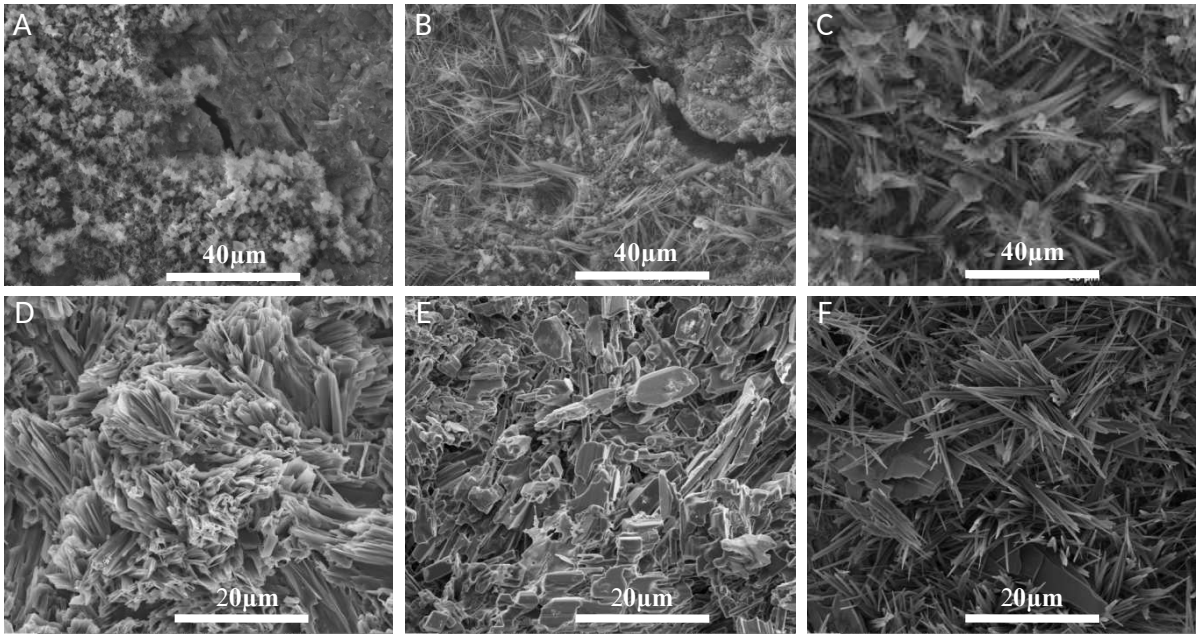

Figure 6 – Scanning electron microscopy using secondary electron images of efflorescence products formed on the surface of geopolymers samples synthesized at different conditions: A: geopolymer MA 1.0, B: geopolymer MA 0.5, C: geopolymer MA 0.0, D: crystallized activator solution MA 1.0, E: dried activator solution MA 0.5, F: dried activator solution MA 0.0.

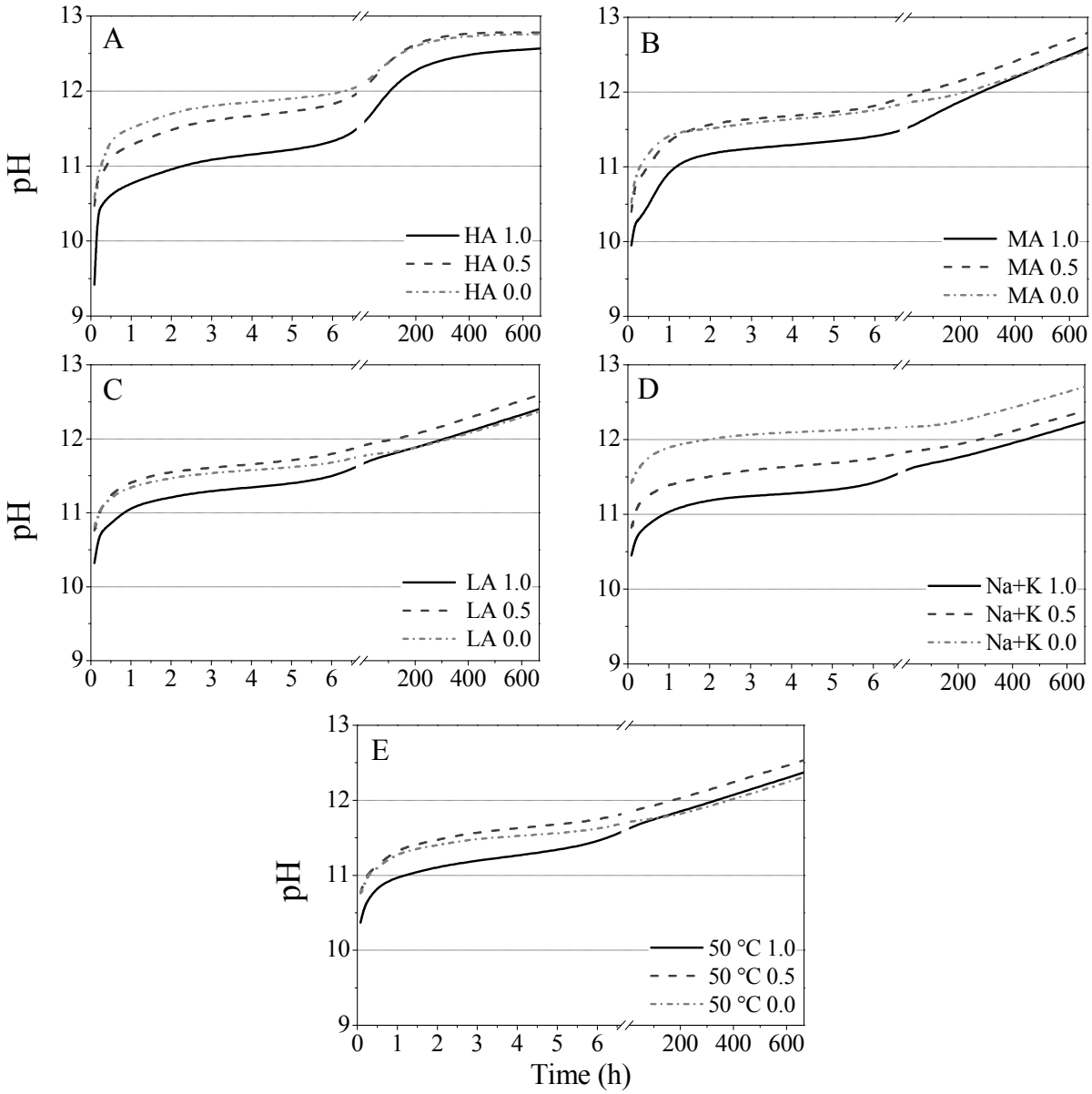

Figure 7 – pH values of the solutions in which each geopolymer system was immersed over time: A. 25% Na_2O, B. 20% Na_2O, C. 15% Na_2O, D. 20% Na_2O + K_2O and E. 20% Na_2O + thermal curing 50°C. Note that the apparent inflection in the data curves are an artefact of the break in the scale on the horizontal axis.

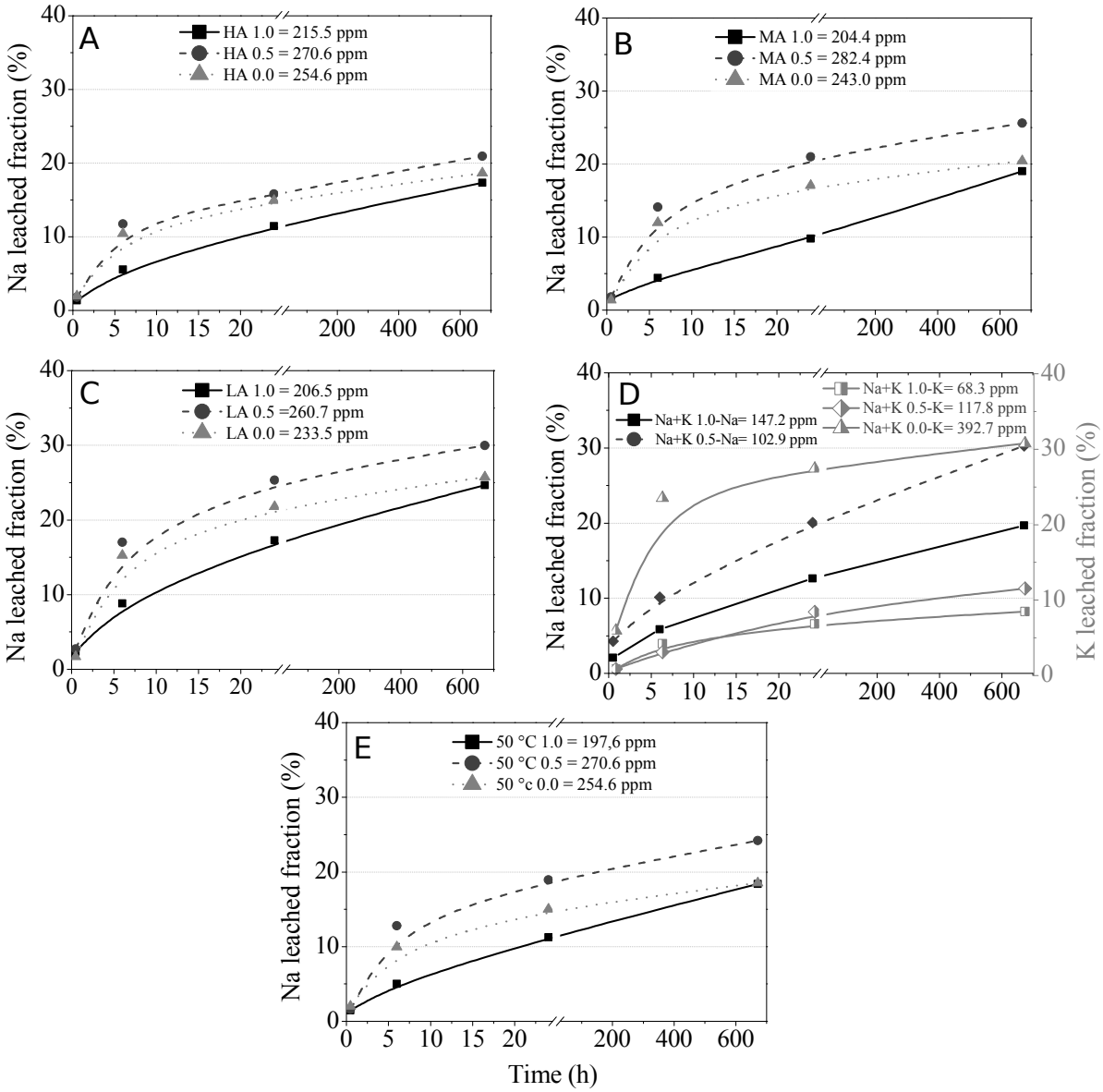

Figure 8 – Concentration of Na^+ and K^+ measured using atomic absorption spectroscopy: A. 25% Na_2O, B. 20% Na_2O, C. 15% Na_2O, D. 20% Na_2O + K_2O and E. 20% Na_2O + thermal curing 50 °C.

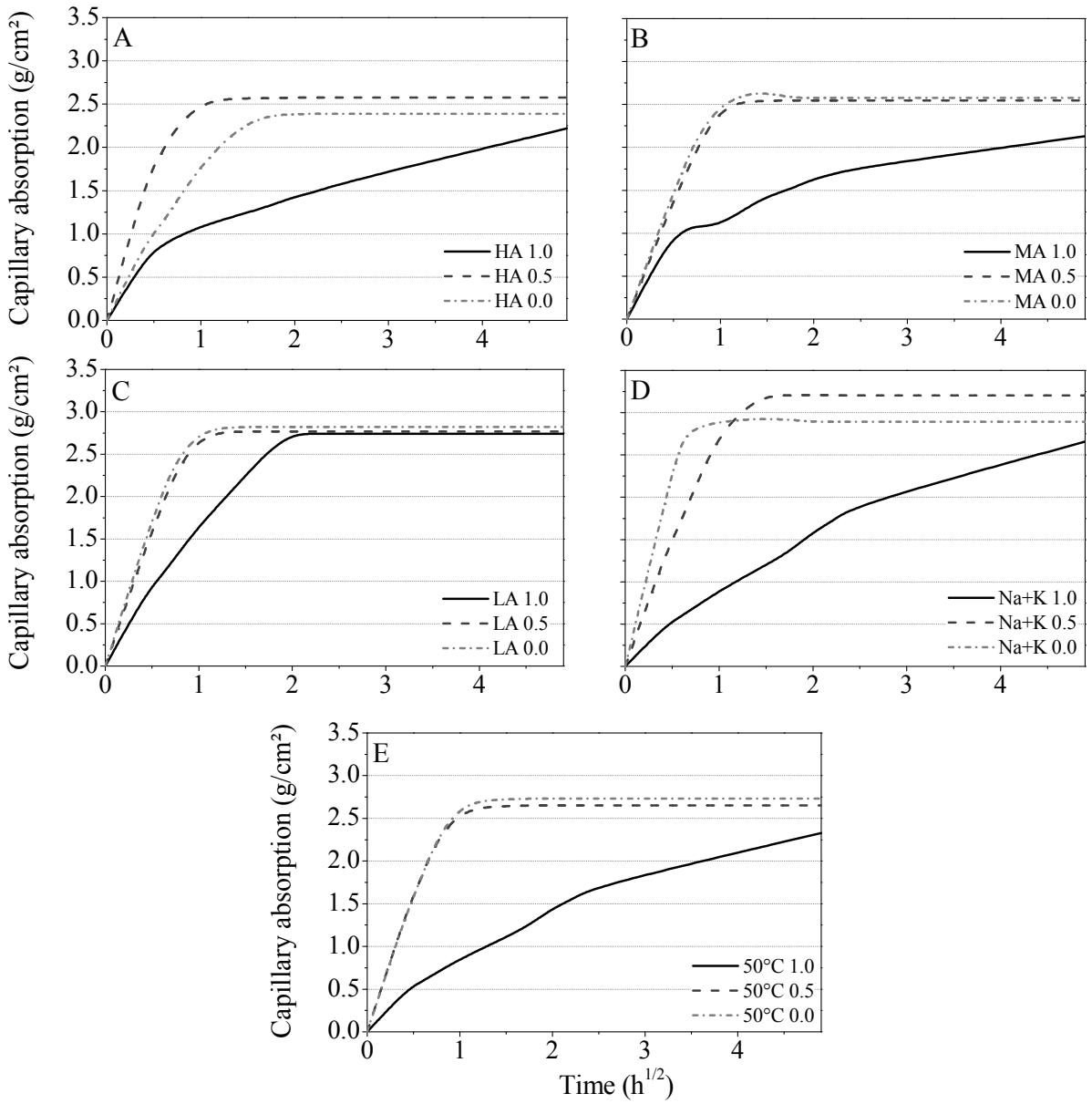

Figure 9 - Capillarity absorption of geopolymers after 28 days of curing: A. 25% Na_2O, B. 20% Na_2O, C. 15% Na_2O, D. 20% Na_2O + K_2O and E. 20% Na_2O + thermal curing 50 °C.

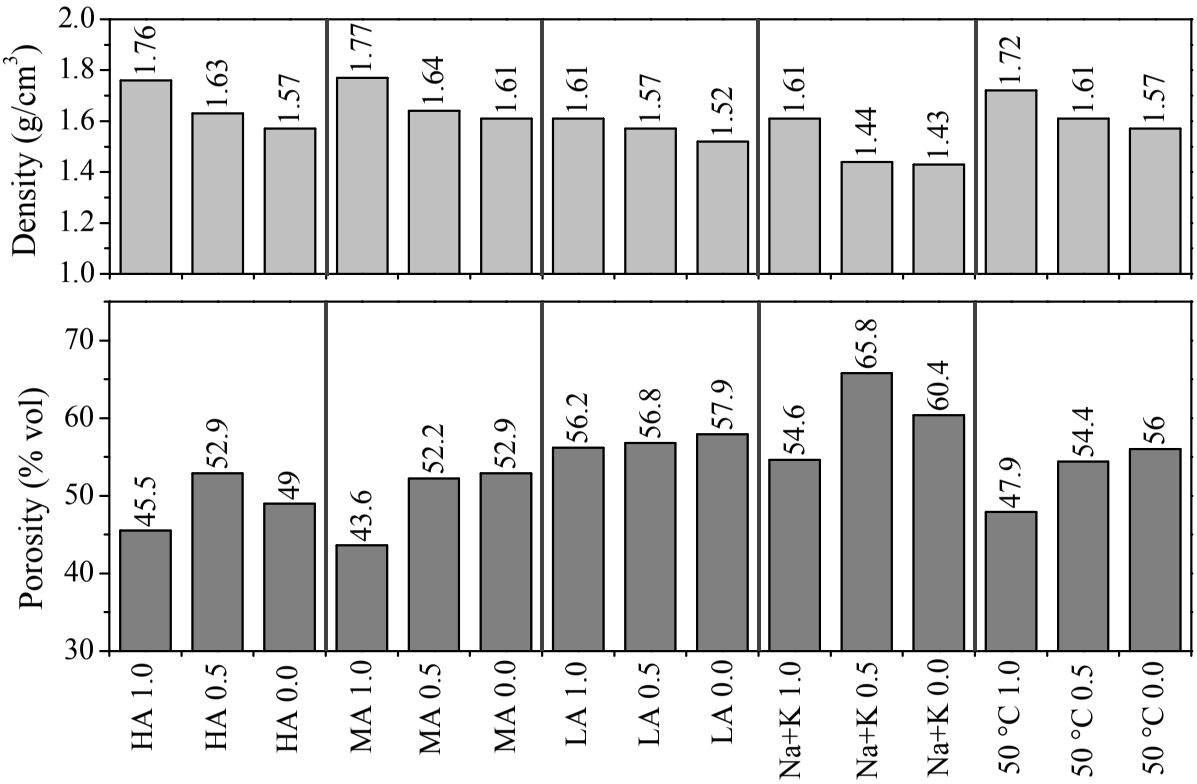

Figure 10 - Density and porosity of geopolymers with 28 days of curing.

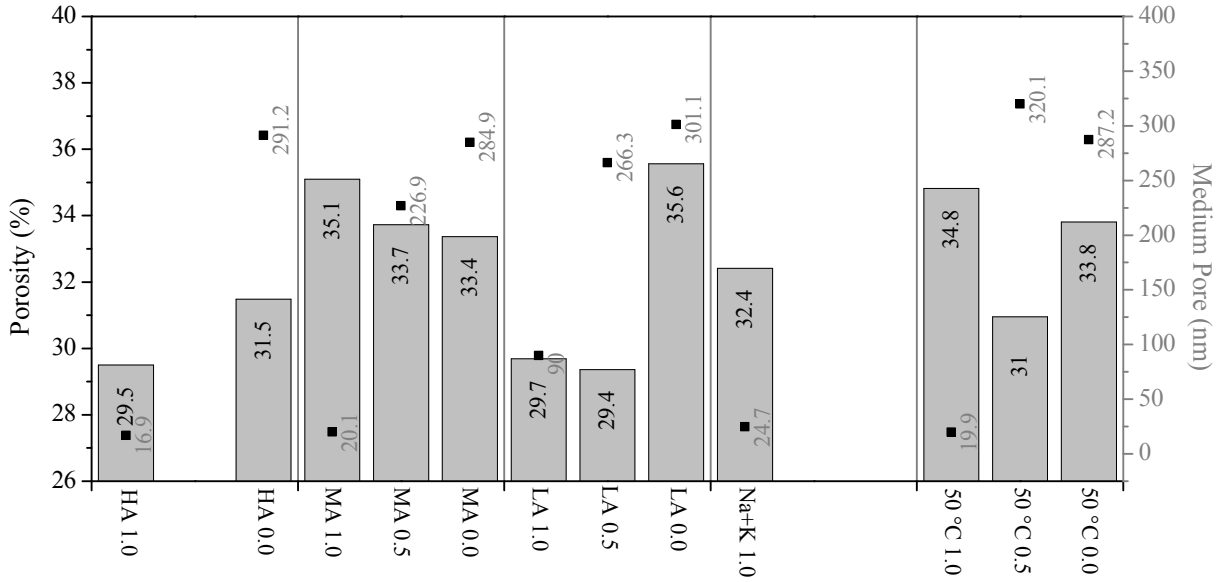

Figure 11 – Porosity and mean pore size of the geopolymers determined by Mercury intrusion porosimetry (MIP).

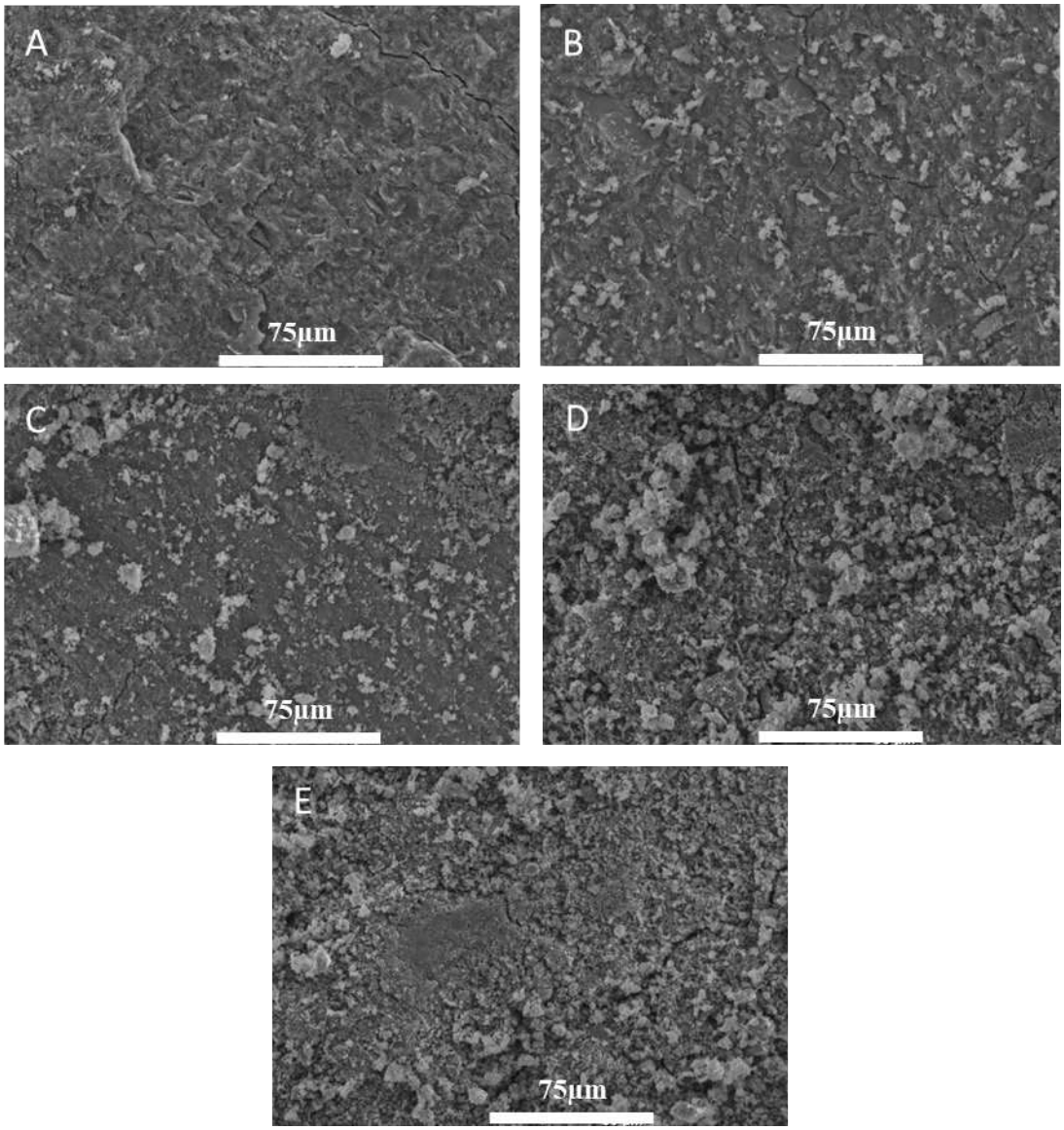

Figure 12 – Scanning electron microscopy by secondary electron images of geopolymers a) HA 1.0, (b) MA 1.0, (c) LA 1.0, (d) MA 0.5, (e) MA 0.0.

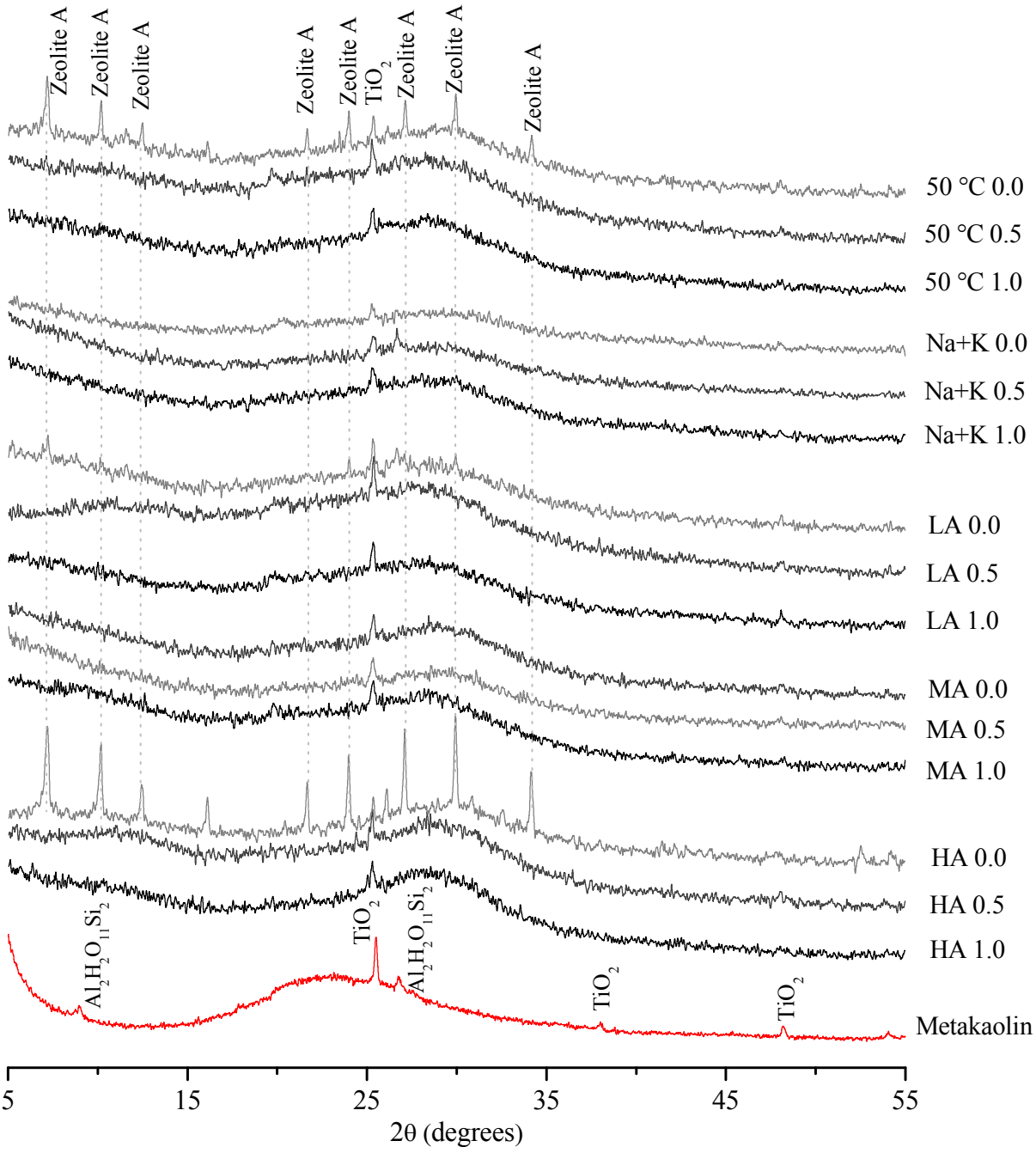

Figure 13 – X-ray diffraction data of metakaolin and the geopolymers systems.

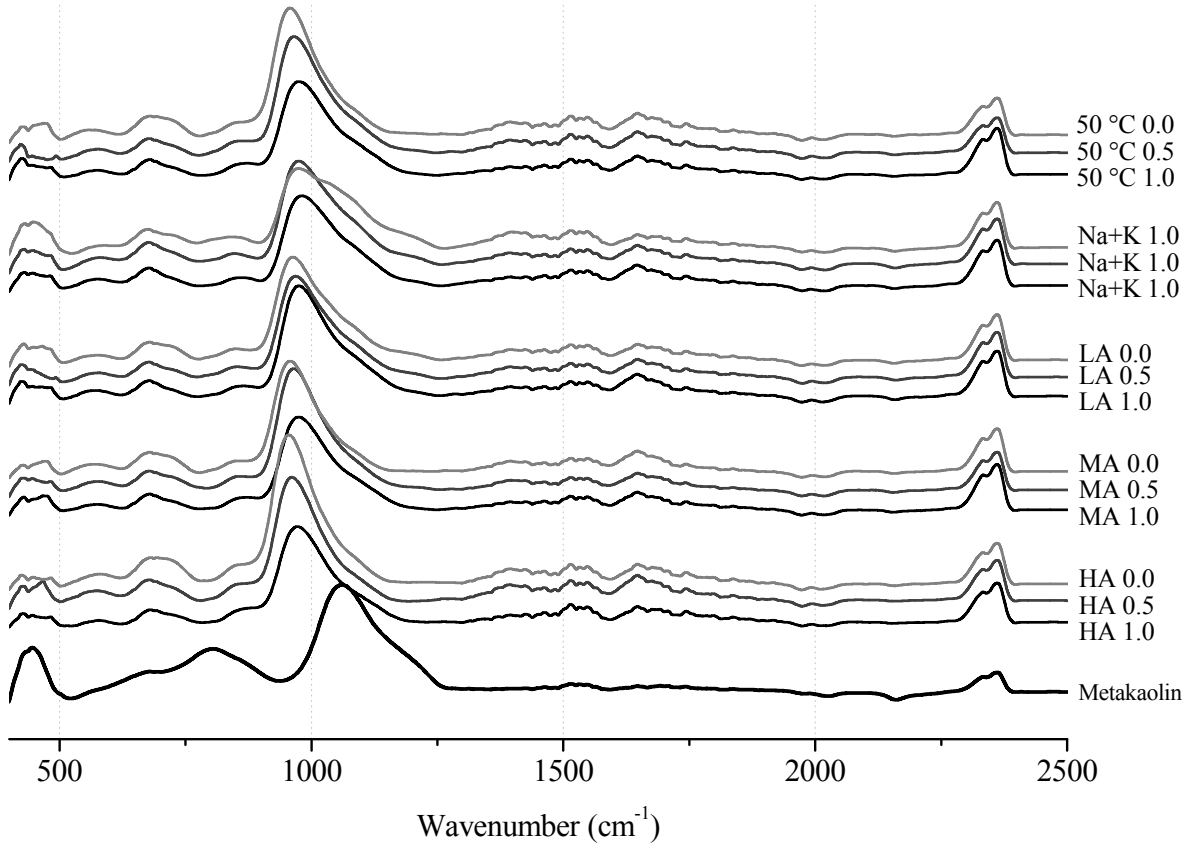

Figure 14 – FTIR spectra of metakaolin and each geopolymer system between 400 and 2500 cm^{-1}.

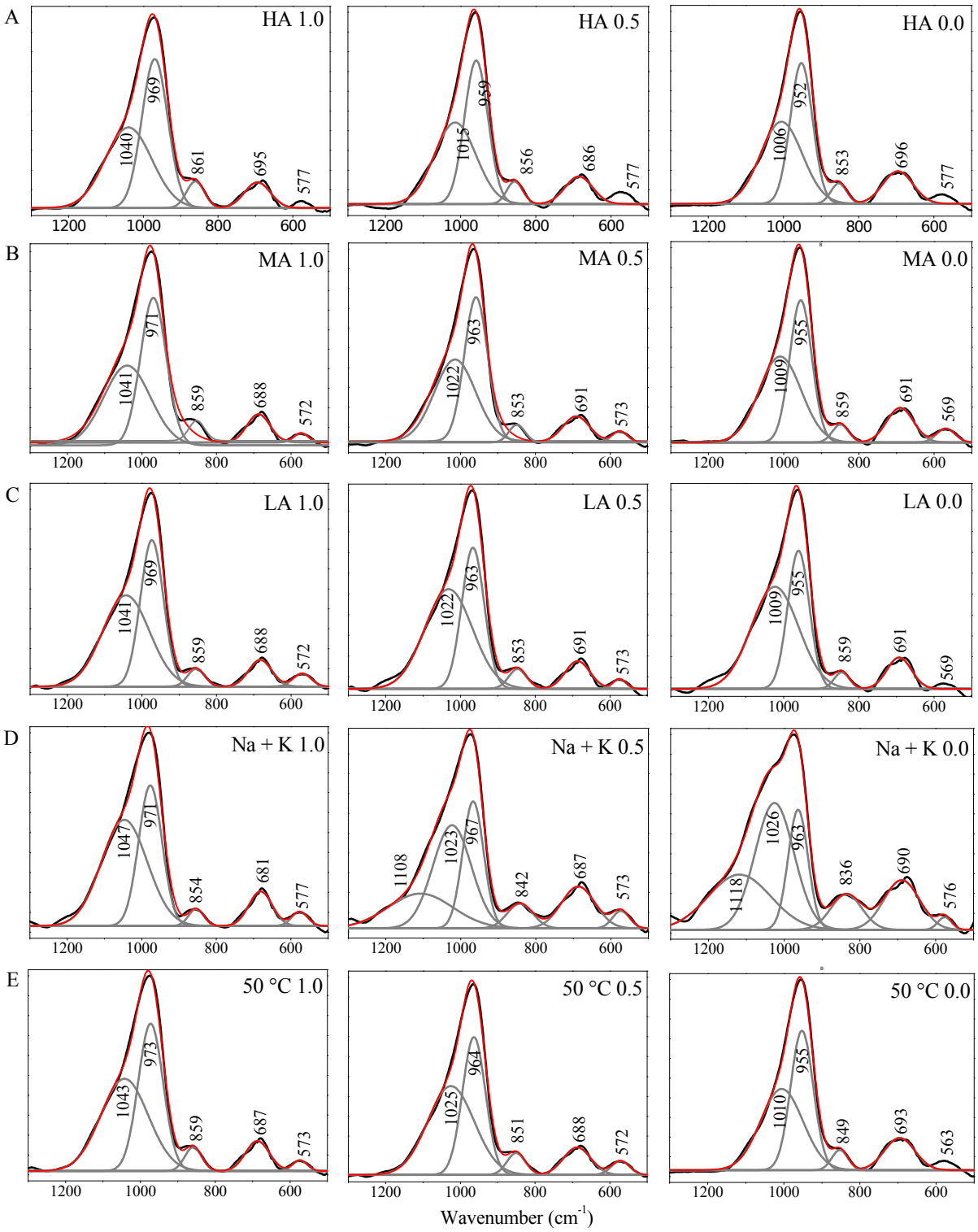

Figure 15 – Fourier transform infrared spectroscopy data (black line) and associated deconvolutions for each geopolymers system: A. 25% Na_2O, B. 20% Na_2O, C. 15% Na_2O, D. 20% Na_2O + K_2O and E. 20% Na_2O + thermal curing 50 °C. The red line is the simulated spectrum, and the grey lines are the fitted peaks.

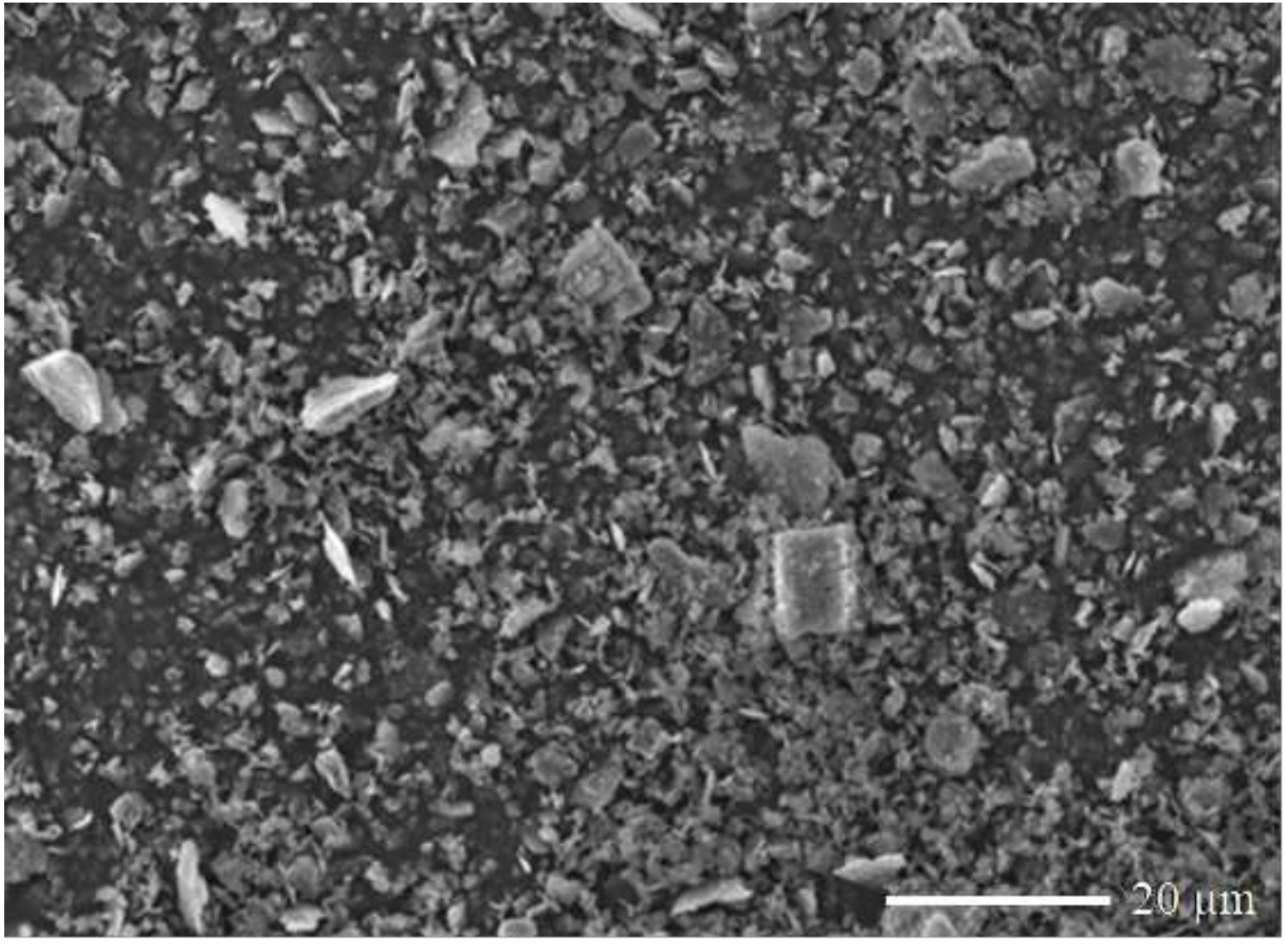
20 μm

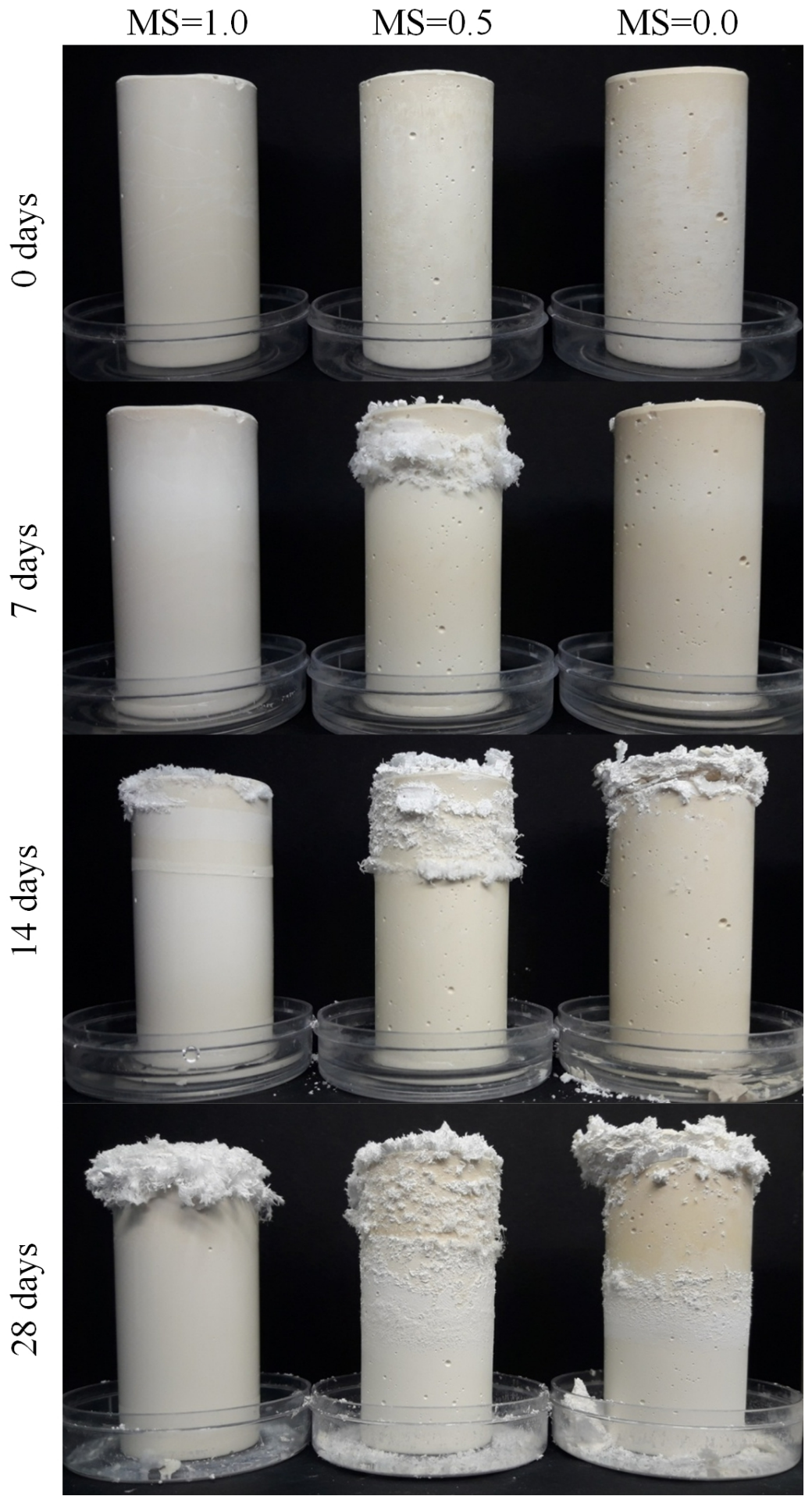
MS=1.0
MS=0.5
MS=0.0
0 days
7 days
14 days
28 days

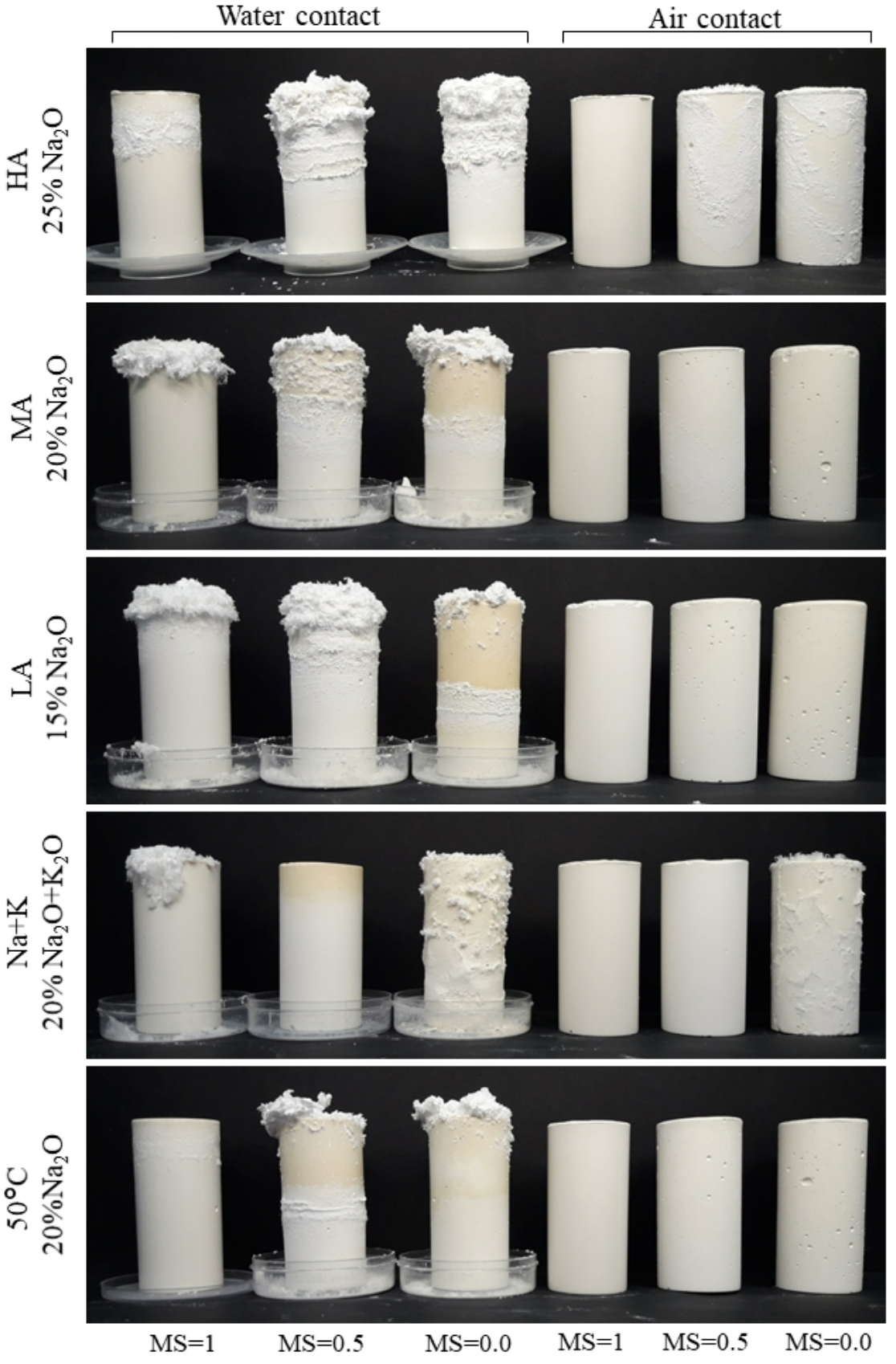
Water contact
Air contact
HA
25% Na_2O
MA
20% Na_2O
LA
15% Na_2O
Na+K
20% Na_2O+K_2O
50°C
20%Na_2O
MS=1
MS=0.5
MS=0.0
MS=1
MS=0.5
MS=0.0

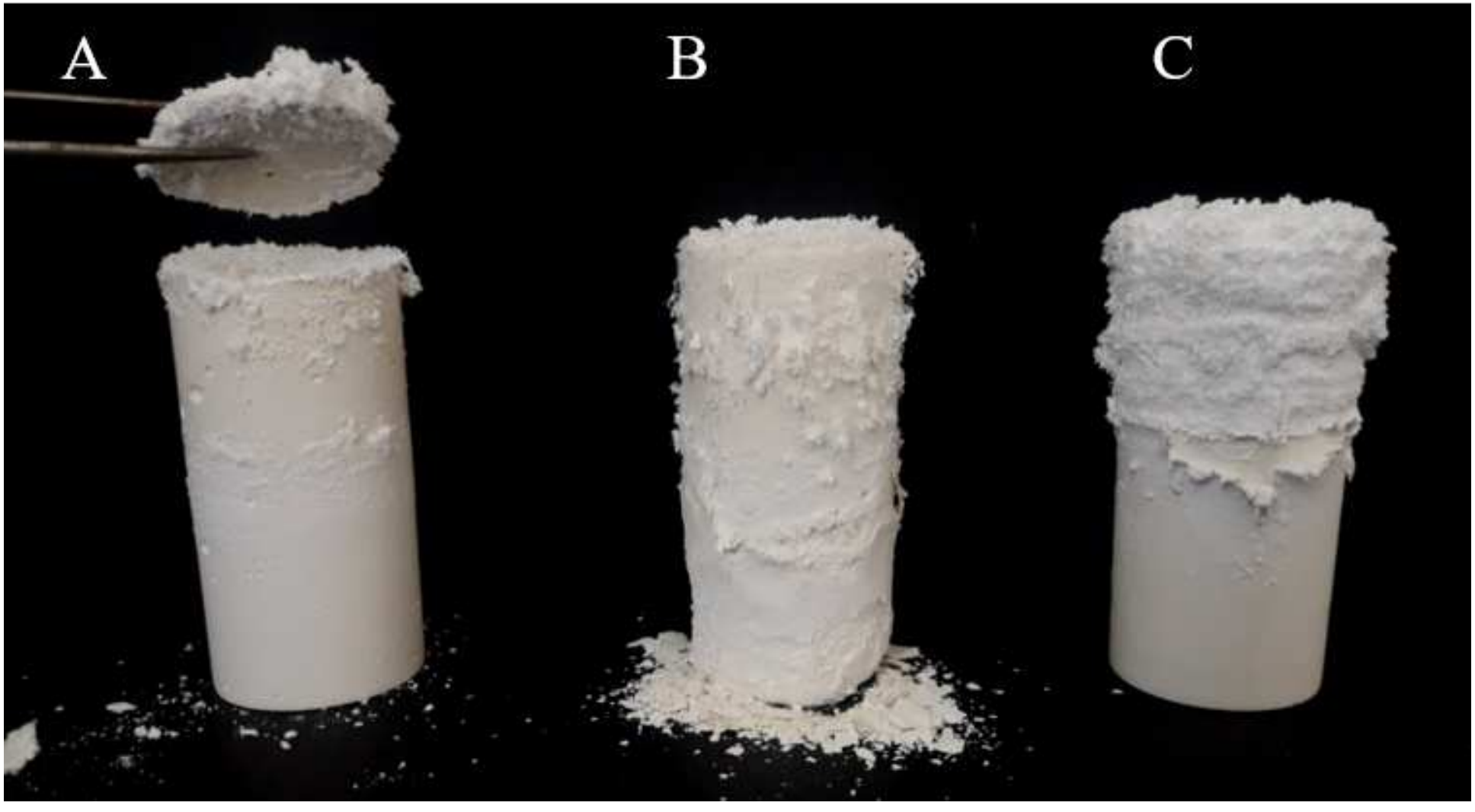
A
B
C

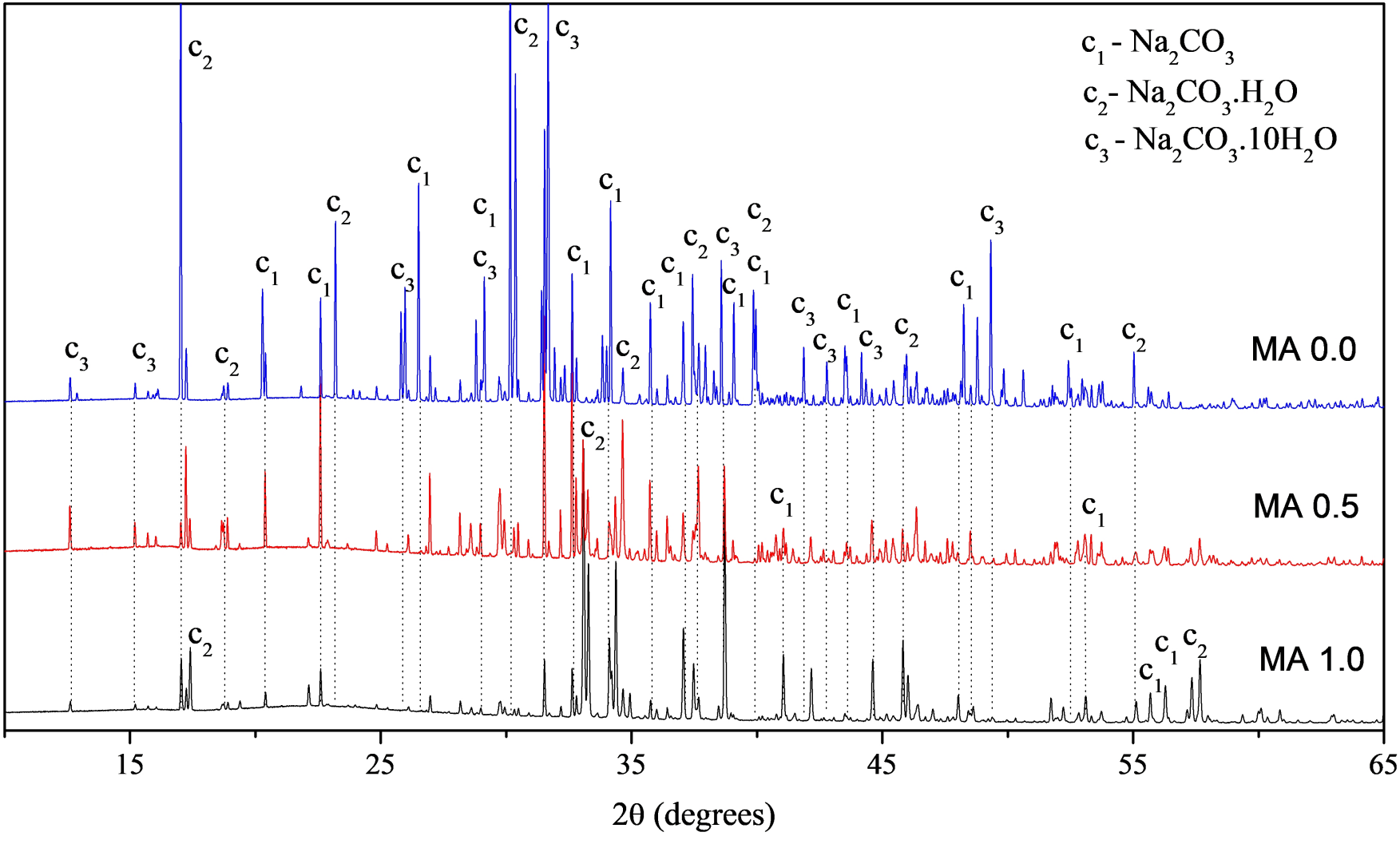
c1 - Na2CO3
c2- Na2CO3.H2O
c3 - Na2CO3.10H2O
MA 0.0
MA 0.5
MA 1.0
15
25
35
45
55
65
2θ (degrees)

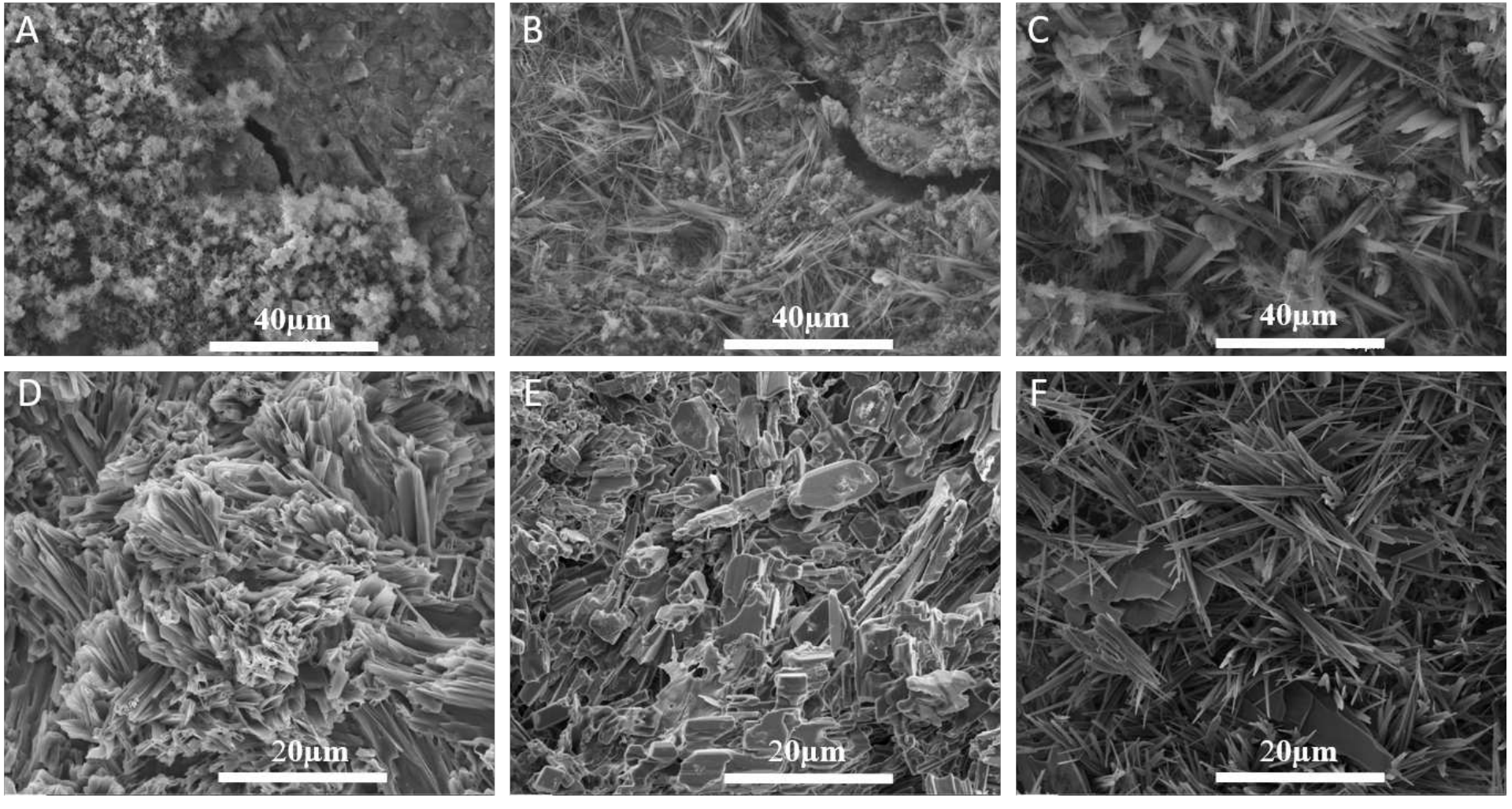
A
40μm
B
40μm
C
40μm
D
20μm
E
20μm
F
20μm

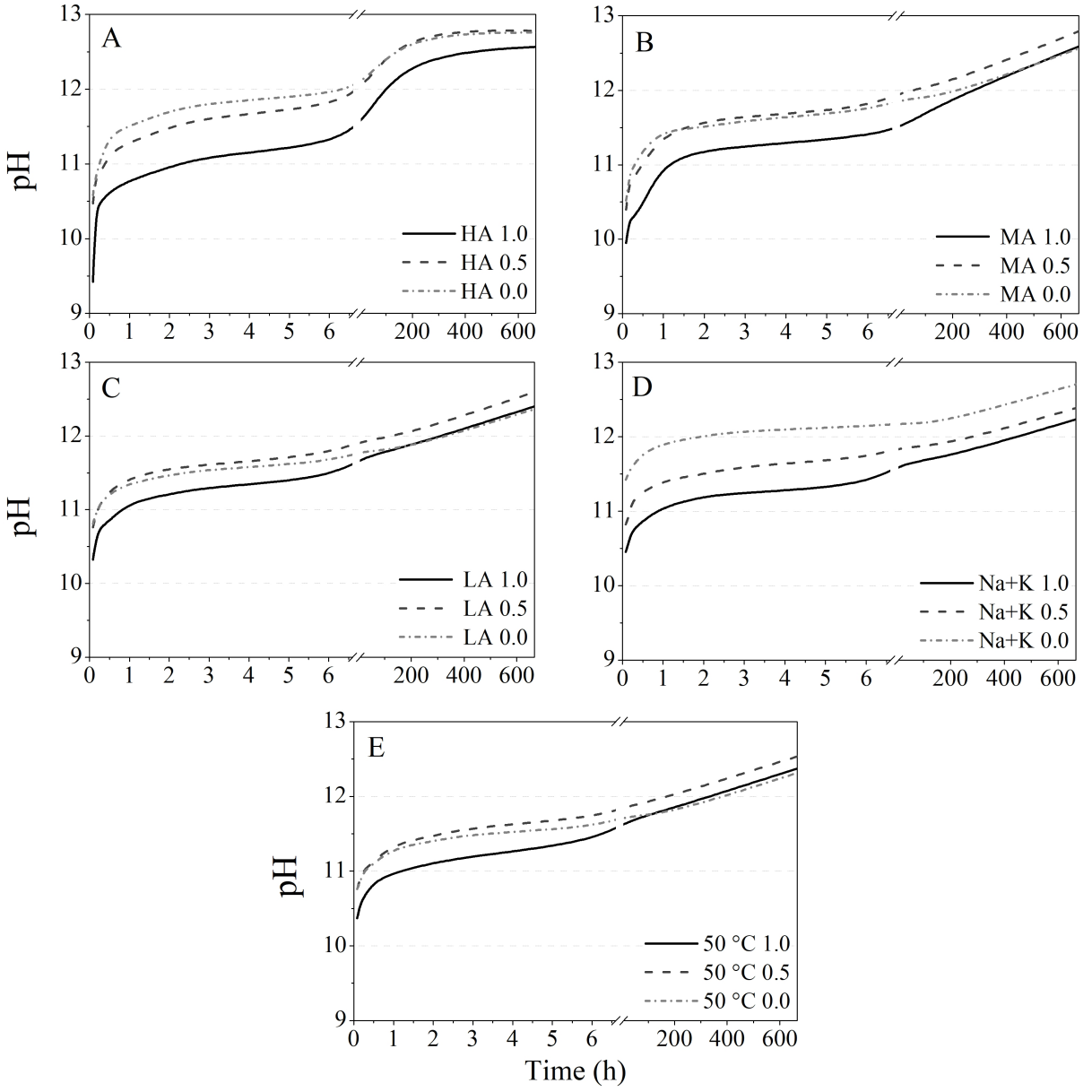
A
HA 1.0
HA 0.5
HA 0.0
B
MA 1.0
MA 0.5
MA 0.0
C
LA 1.0
LA 0.5
LA 0.0
D
Na+K 1.0
Na+K 0.5
Na+K 0.0
E
50 °C 1.0
50 °C 0.5
50 °C 0.0
pH
Time (h)

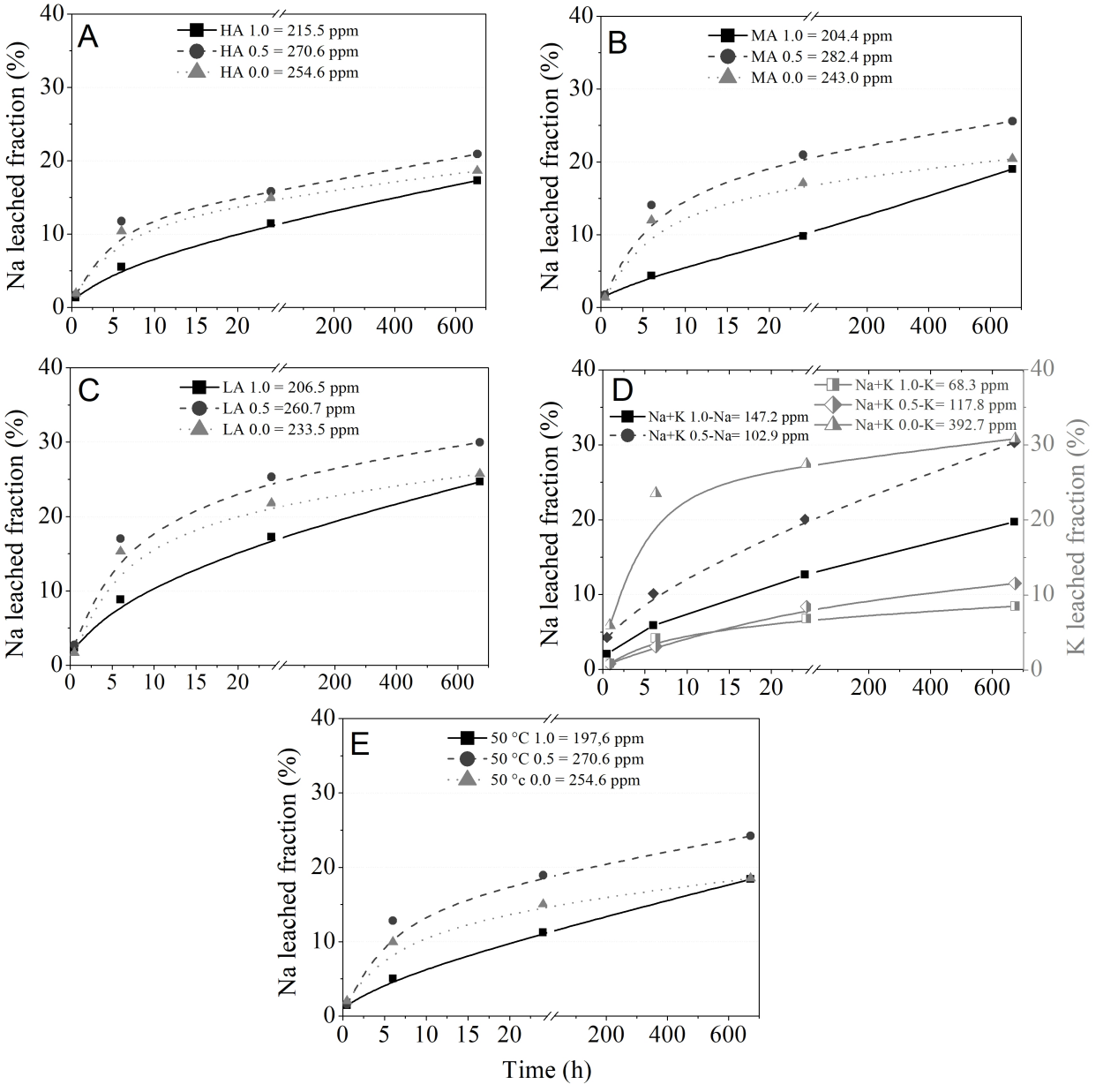
A
HA 1.0 = 215.5 ppm
HA 0.5 = 270.6 ppm
HA 0.0 = 254.6 ppm
B
MA 1.0 = 204.4 ppm
MA 0.5 = 282.4 ppm
MA 0.0 = 243.0 ppm
C
LA 1.0 = 206.5 ppm
LA 0.5 =260.7 ppm
LA 0.0 = 233.5 ppm
D
Na+K 1.0-Na= 147.2 ppm
Na+K 0.5-Na= 102.9 ppm
Na+K 1.0-K= 68.3 ppm
Na+K 0.5-K= 117.8 ppm
Na+K 0.0-K= 392.7 ppm
K leached fraction (%)
E
50 °C 1.0 = 197,6 ppm
50 °C 0.5 = 270.6 ppm
50 °c 0.0 = 254.6 ppm
Na leached fraction (%)
Time (h)

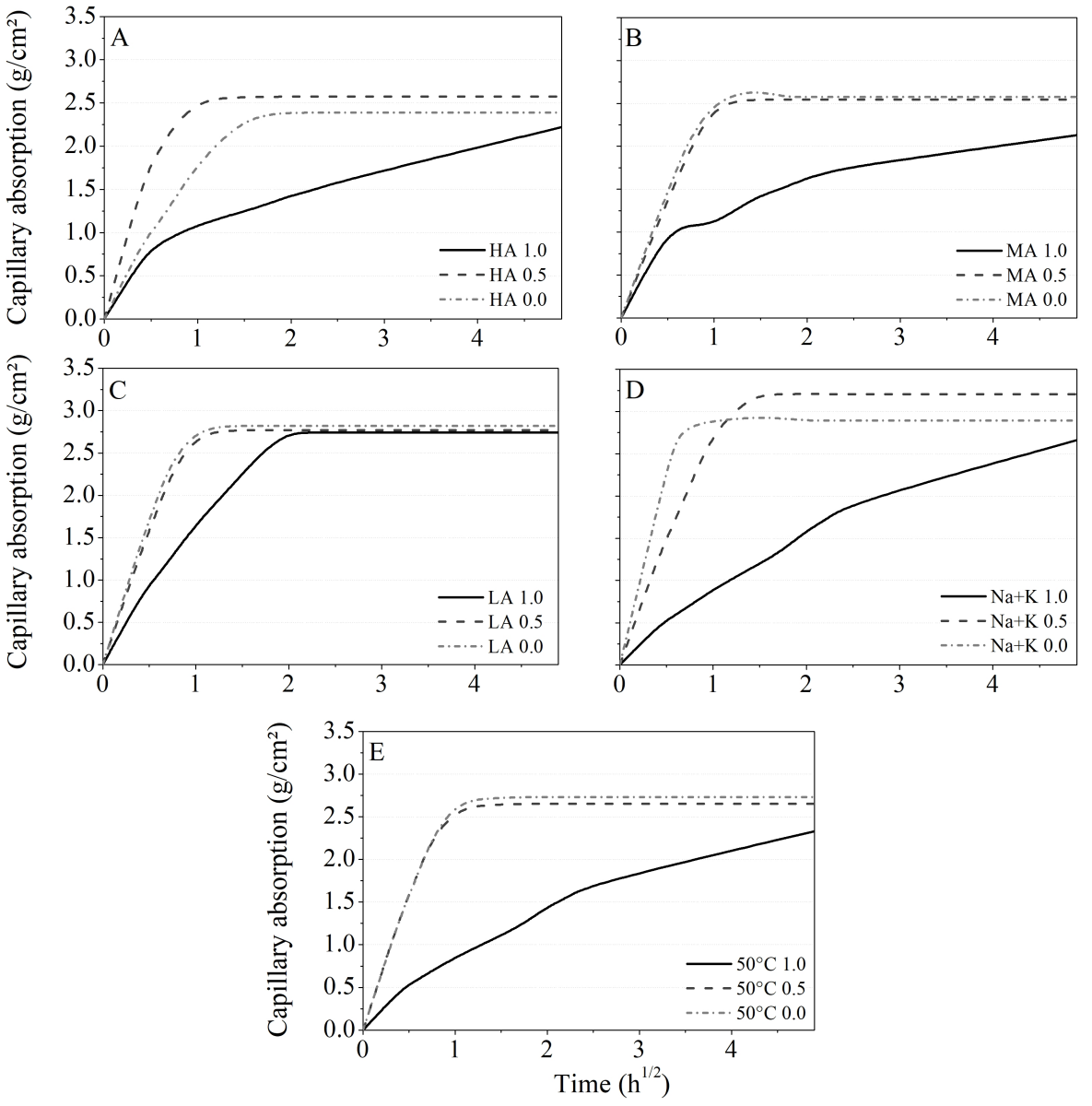
A
HA 1.0
HA 0.5
HA 0.0
B
MA 1.0
MA 0.5
MA 0.0
C
LA 1.0
LA 0.5
LA 0.0
D
Na+K 1.0
Na+K 0.5
Na+K 0.0
E
50°C 1.0
50°C 0.5
50°C 0.0
Capillary absorption (g/cm²)
Time (h^1/2)

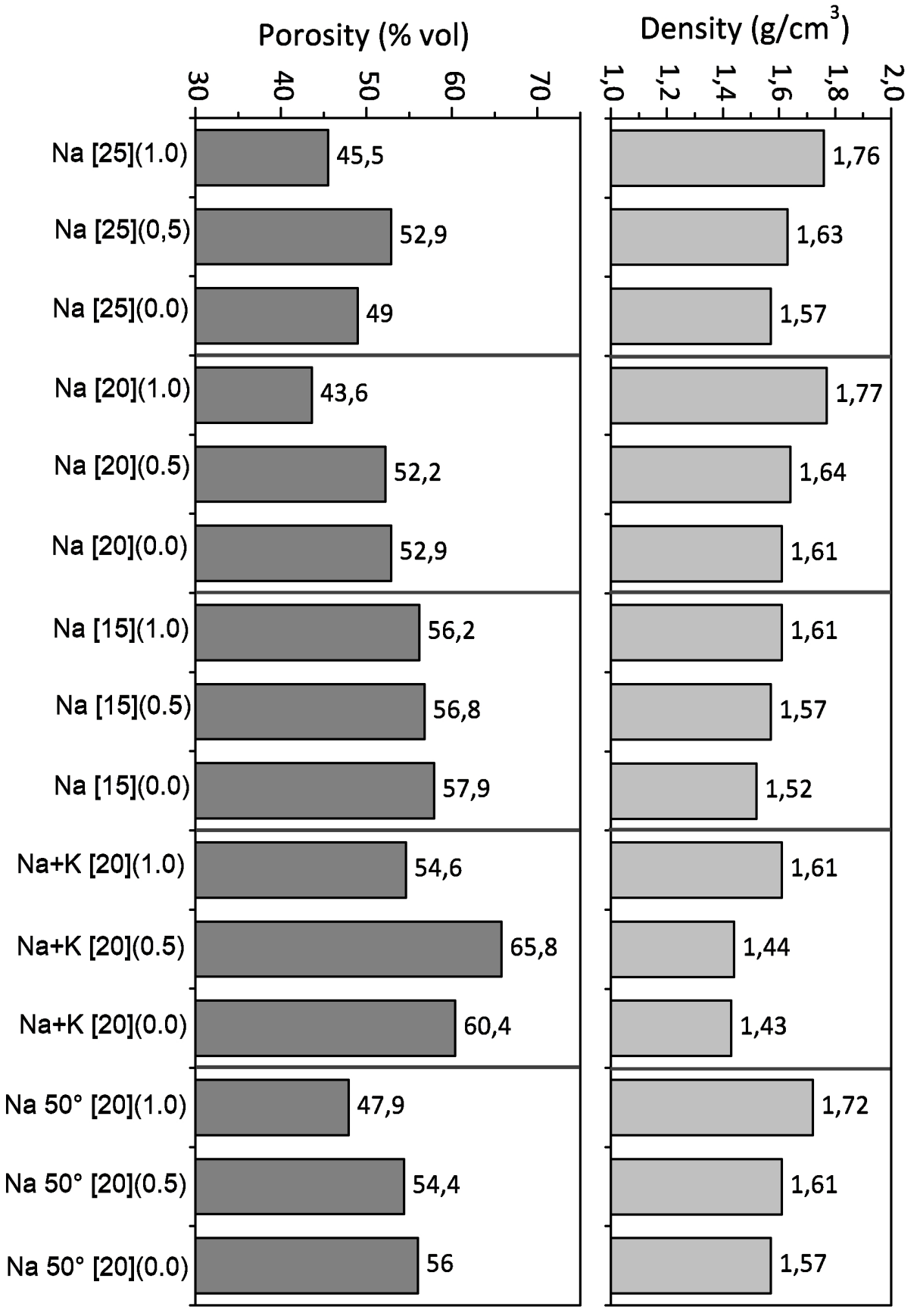
Porosity (% vol)
30
40
50
60
70
Density (g/cm3)
1,0
1,2
1,4
1,6
1,8
2,0
Na [25](1.0)
45,5
1,76
Na [25](0,5)
52,9
1,63
Na [25](0.0)
49
1,57
Na [20](1.0)
43,6
1,77
Na [20](0.5)
52,2
1,64
Na [20](0.0)
52,9
1,61
Na [15](1.0)
56,2
1,61
Na [15](0.5)
56,8
1,57
Na [15](0.0)
57,9
1,52
Na+K [20](1.0)
54,6
1,61
Na+K [20](0.5)
65,8
1,44
Na+K [20](0.0)
60,4
1,43
Na 50° [20](1.0)
47,9
1,72
Na 50° [20](0.5)
54,4
1,61
Na 50° [20](0.0)
56
1,57

Porosity (%)
Medium Pore (nm)
40
38
36
34
32
30
28
26
400
350
300
250
200
150
100
50
0
29.5
16.9
31.5
291.2
35.1
20.1
33.7
226.9
33.4
284.9
29.7
90
29.4
266.3
35.6
301.1
32.4
24.7
34.8
19.9
31
320.1
33.8
287.2
HA 1.0
HA 0.0
MA 1.0
MA 0.5
MA 0.0
LA 1.0
LA 0.5
LA 0.0
Na+K 1.0
50 °C 1.0
50 °C 0.5
50 °C 0.0

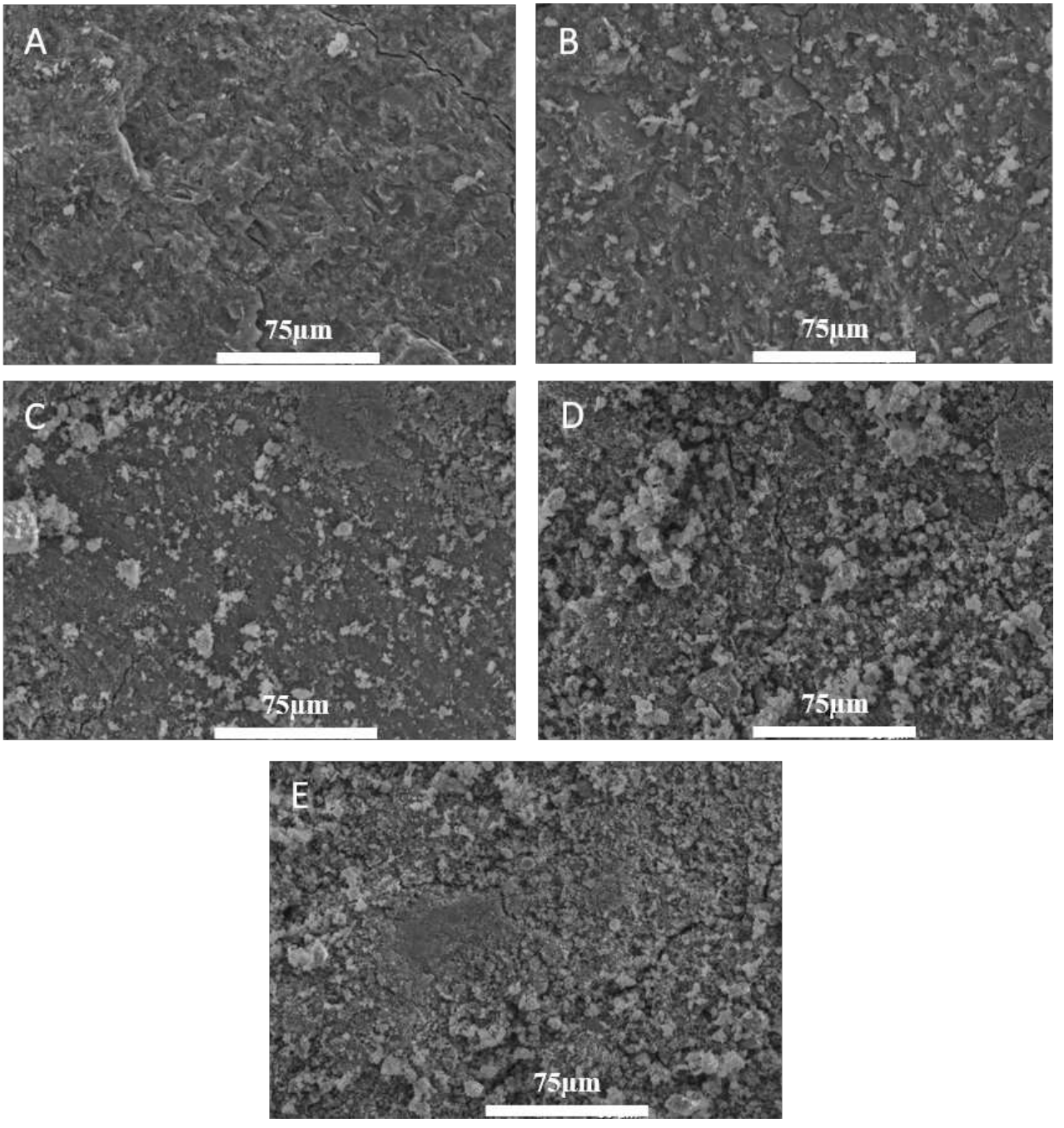
A
75µm
B
75µm
C
75µm
D
75µm
E
75µm

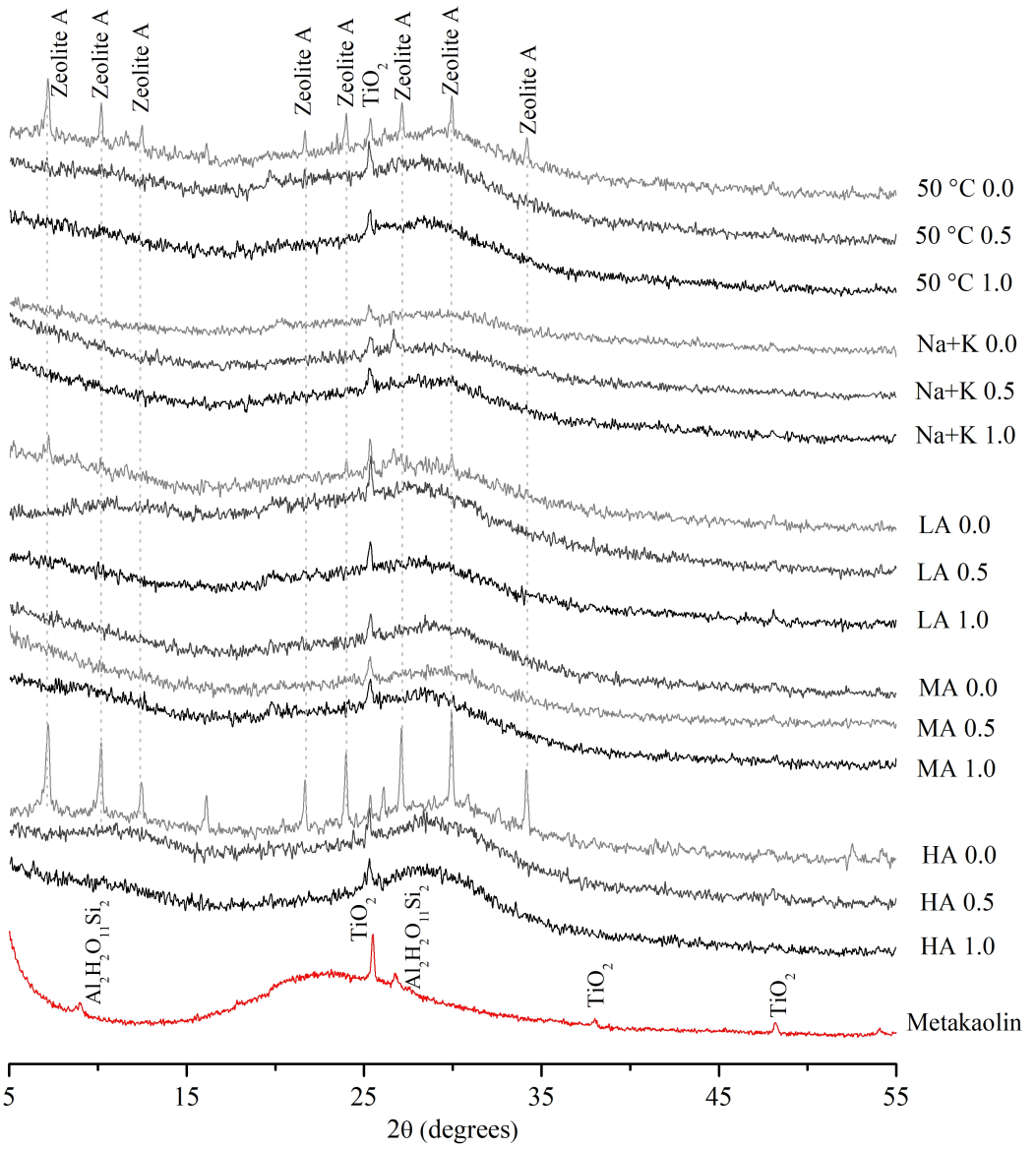
Zeolite A
Zeolite A
Zeolite A
Zeolite A
Zeolite A
TiO2
Zeolite A
Zeolite A
Zeolite A
50 °C 0.0
50 °C 0.5
50 °C 1.0
Na+K 0.0
Na+K 0.5
Na+K 1.0
LA 0.0
LA 0.5
LA 1.0
MA 0.0
MA 0.5
MA 1.0
HA 0.0
HA 0.5
HA 1.0
Al2H2O11Si2
TiO2
Al2H2O11Si2
TiO2
TiO2
Metakaolin
5
15
25
35
45
55
2θ (degrees)

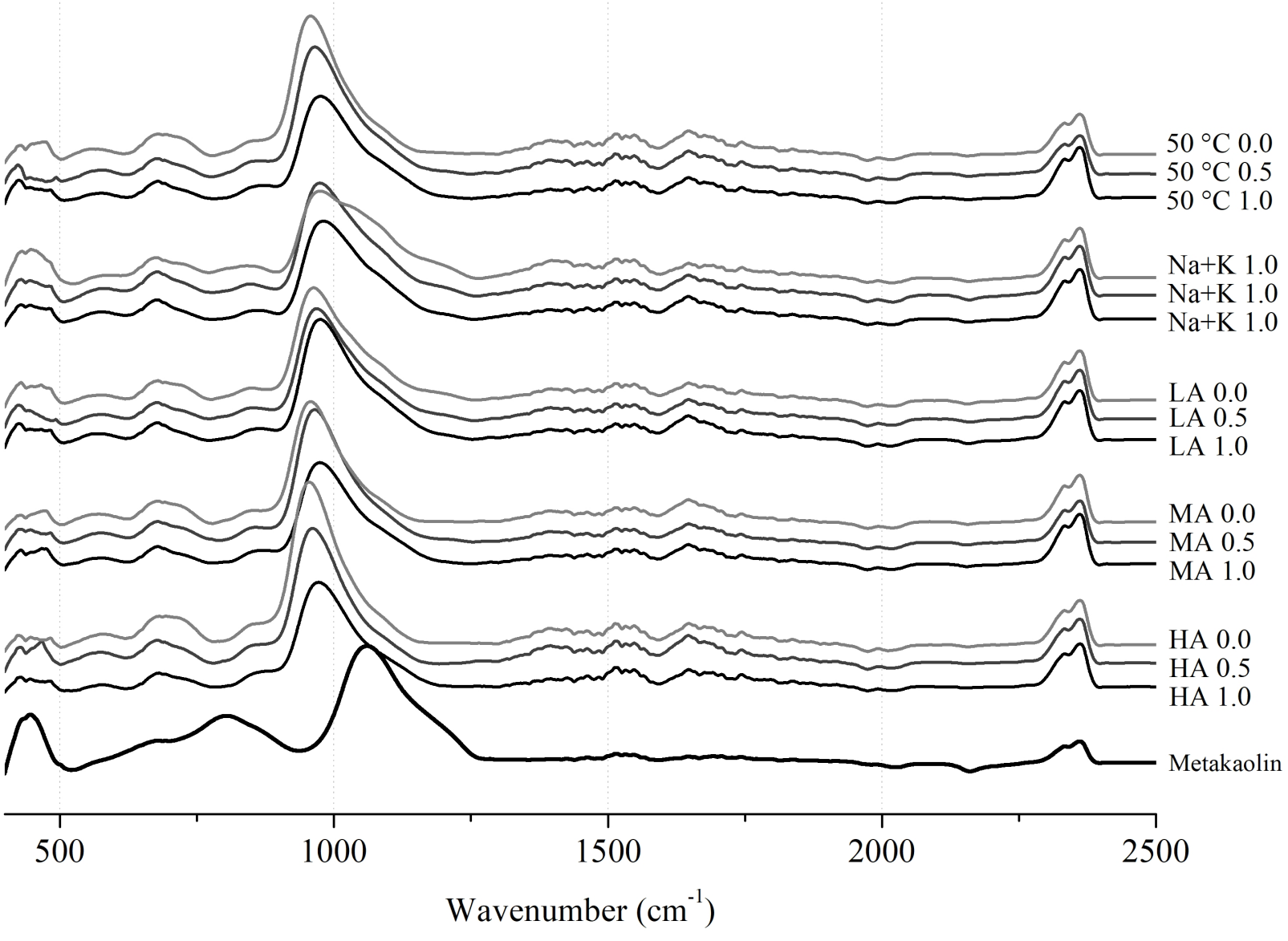
50 °C 0.0
50 °C 0.5
50 °C 1.0
Na+K 1.0
Na+K 1.0
Na+K 1.0
LA 0.0
LA 0.5
LA 1.0
MA 0.0
MA 0.5
MA 1.0
HA 0.0
HA 0.5
HA 1.0
Metakaolin
500
1000
1500
2000
2500
Wavenumber (cm-1)

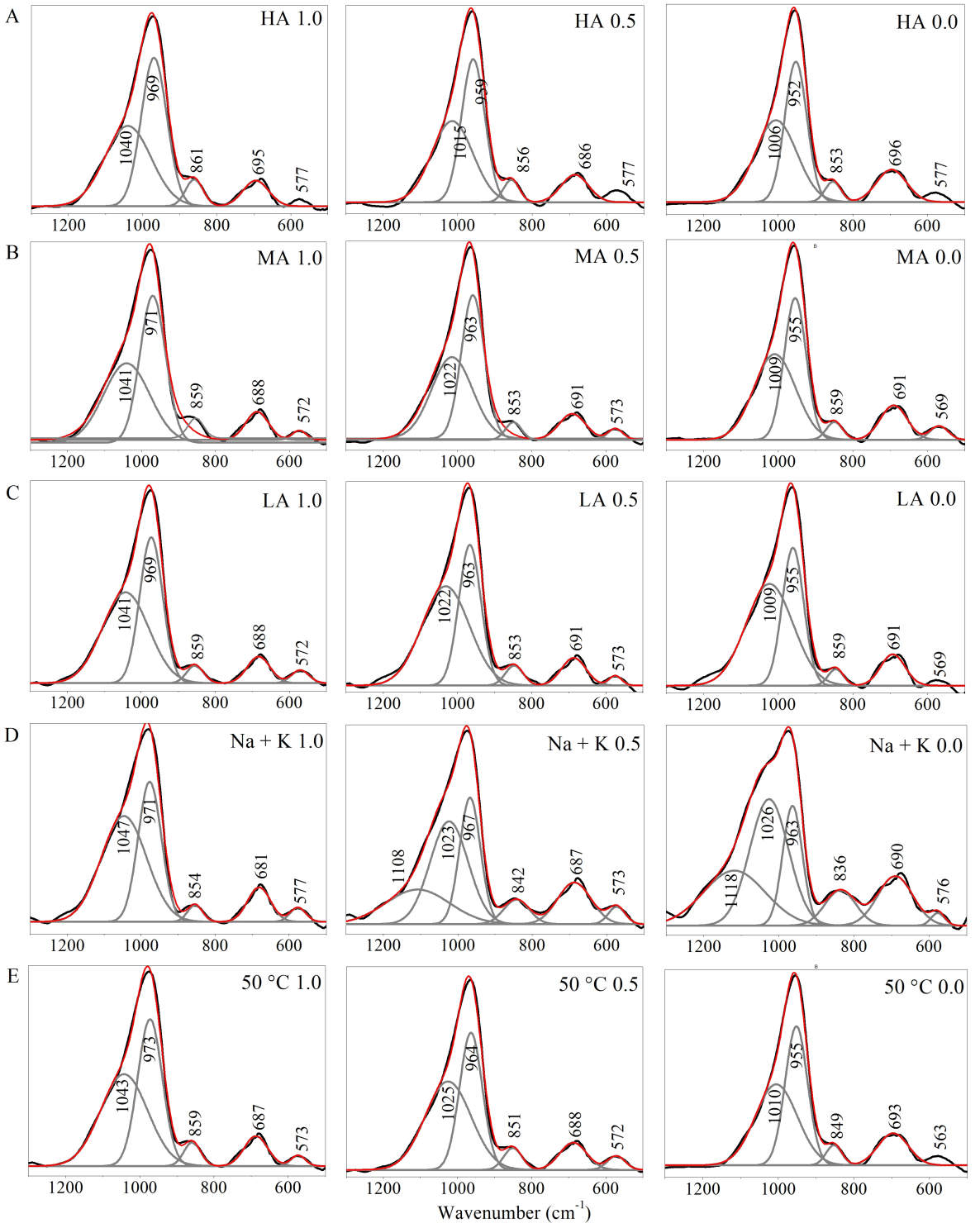
A
HA 1.0
1040
969
861
695
577
HA 0.5
1015
959
856
686
577
HA 0.0
1006
952
853
696
577
B
MA 1.0
1041
971
859
688
572
MA 0.5
1022
963
853
691
573
MA 0.0
1009
955
859
691
569
C
LA 1.0
1041
969
859
688
572
LA 0.5
1022
963
853
691
573
LA 0.0
1009
955
859
691
569
D
Na + K 1.0
1047
971
854
681
577
Na + K 0.5
1108
1023
967
842
687
573
Na + K 0.0
1118
1026
963
836
690
576
E
50 °C 1.0
1043
973
859
687
573
50 °C 0.5
1025
964
851
688
572
50 °C 0.0
1010
955
849
693
563
1200
1000
800
600
Wavenumber (cm-1)

Declaration of interests

 The authors declare that they have no known competing financial interests or personal relationships that could have appeared to influence the work reported in this paper.

The authors declare the following financial interests/personal relationships which may be considered as potential competing interests: